arXiv:2309.13382v1 [astro-ph.HE] 23 Sep 2023

Magnetic Reconnection and Associated Particle Acceleration in High-energy Astrophysics

Fan Guo[1*], Yi-Hsin Liu[2], Seiji Zenitani[3*] and Masahiro Hoshino[4]

[1]Los Alamos National Laboratory, Los Alamos, New Mexico 87545, USA.
[2]Department of Physics and Astronomy, Dartmouth College, Hanover, New Hampshire 03755, USA.
[3]Space Research Institute, Austrian Academy of Sciences, Schmiedlstraße 6, 8042 Graz, Austria.
[4]Department of Earth and Planetary Science, The University of Tokyo, Tokyo, 113-0033, Japan.

*Corresponding author(s). E-mail(s): guofan@lanl.gov; seiji.zenitani@oeaw.ac.at;
Contributing authors: yi-hsin.liu@dartmouth.edu; hoshino@eps.s.u-tokyo.ac.jp;

Abstract

Magnetic reconnection occurs ubiquitously in the universe and is often invoked to explain fast energy release and particle acceleration in high-energy astrophysics. The study of relativistic magnetic reconnection in the magnetically dominated regime has surged over the past two decades, revealing the physics of fast magnetic reconnection and nonthermal particle acceleration. Here we review these recent progresses, including the magnetohydrodynamic and collisionless reconnection dynamics as well as particle energization. The insights in astrophysical reconnection strongly connect to the development of magnetic reconnection in other areas, and further communication is greatly desired. We also provide a summary and discussion of key physics processes and frontier problems, toward a better understanding to the roles of magnetic reconnection in high-energy astrophysics.

Keywords: magnetic reconnection, particle acceleration, high-energy astrophysics

Contents

1 Introduction

Magnetic reconnection is a ubiquitous process that occurs in many space, solar, astrophysical, and laboratory systems. It was initially proposed to explain the fast energy release and acceleration of particles in space and astrophysical systems (e.g., Parker, 1957; Sweet, 1958; Petschek, 1964). During reconnection, magnetic topology changes lead to rapid release of magnetic energy in highly conducting plasmas that cannot be explained by magnetic diffusion. Magnetic reconnection is now widely considered as a pivotal process for explosive energy release, high-energy particle acceleration and radiation in the universe (Uzdensky, 2011; Hoshino and Lyubarsky, 2012; Arons, 2012; Blandford et al, 2017; Guo et al, 2020; Ji et al, 2022).

In high-energy astrophysics, magnetic reconnection can occur in pulsar wind nebulae (PWNe) and pulsar magnetosphere, relativistic jets of active galactic nuclei (AGNs) and gamma-ray bursts, accretion disks and coronae surrounding massive compact objects, as well as strong magnetic field regions in magnetars, etc. (see Section 1.1 for a more extensive discussion). The reconnection region is expected to be much larger than the kinetic scale so a magnetohydrodynamic (MHD) description is necessary. However, many regimes of high-Lundquist-number magnetic reconnection show multiple X-lines and flux ropes (islands in 2D) develop as the secondary tearing instability is active in a current layer. Kinetic processes are important in a collisionless system (Daughton and Karimabadi, 2007; Guo et al, 2015; Sironi et al, 2016) or when a hierarchy of collisional plasmoids (Biskamp, 1986; Shibata and Tanuma, 2001a; Loureiro et al, 2007; Bhattacharjee et al, 2009; Uzdensky et al, 2010) develop kinetic-scale current layers that may trigger collisionless reconnection (Daughton et al, 2009; Ji and Daughton, 2011; Stanier et al, 2019). Magnetic reconnection has been proposed as a mechanism to explain a broad range of high-energy astrophysical phenomena and radiation signatures. This includes high-energy radiation flares and their fast variability and polarized emission signature (Zhang et al, 2018, 2020, 2021a, 2022a; Zhang and Giannios, 2021; Petropoulou et al, 2016), as well as emissions from the accretion flows recently observed by the Event Horizon Telescope (EHT) (Ripperda et al, 2020) and fast radio bursts (FRBs) (Philippov et al, 2019).

In many high-energy astrophysical systems, it is often estimated that magnetic reconnection, if occurs, will proceed in a magnetically dominated environment. The parameter for measuring the dominance is the so-called magnetization parameter[1]:

$$\sigma = B^2/(4\pi w) \tag{1}$$

with the enthalpy density $w = nmc^2 + [\Gamma_a/(\Gamma_a - 1)]P$. Here B is the magnitude of magnetic field, n is the proper plasma density, c is the speed of light, Γ_a is the ratio of specific heats, and m and P are the rest mass and proper pressure of the plasma particles under study, which can be the electron-positron pairs or proton-electron pairs, or a mixture of more species. It is

[1] In the nonrelatvistic case, it is more adequate to use plasma β or $\sigma_T = B^2/(6\pi nT)$ to measure the magnetic field dominance. See Drake et al. this collection.

expected that in many situations, σ can be much larger than unit and the Alfvén speed $v_A/c = \sqrt{\sigma/(\sigma+1)}$ is close to the speed of light. In terms of the energy budget, $\sigma_r = B_r^2/(4\pi w)$ is the ratio between the potential free energy carried by the Poynting flux to the particle energy density flux into the reconnection region (B_r represents the reconnecting field component). Analytical theories and MHD simulations have been developed to understand relativistic magnetic reconnection (Section 2). Particle-in-cell (PIC) simulations have greatly enhanced our understanding to relativistic magnetic reconnection in the high-σ regime. Magnetic reconnection has been found to support a fast reconnection rate $R \sim 0.1 - 0.3$, indicating fast energy release (Lyubarsky, 2005; Liu et al, 2015, 2017, 2020; Werner et al, 2018; Goodbred and Liu, 2022). It has been shown to efficiently convert a sizeable fraction of the magnetic energy, leading to a strong particle energization. These reconnection layers are shown to strongly accelerate particles to high energy, leading to power-law energy spectra with spectral index approaching $p \sim 1$ for large σ (Zenitani and Hoshino, 2001; Sironi and Spitkovsky, 2014; Guo et al, 2014, 2015; Werner et al, 2016). The key physics and observational implications of these results are being actively studied. We discuss collisionless reconnection physics, and plasma heating and particle acceleration in relativistic magnetic reconnection in Sections 3 and 4, respectively. In this magnetically-dominated regime, collisionless shocks may be inefficient in dissipating magnetically dominated flows and accelerating energetic particles (e.g., Sironi et al, 2015), magnetic reconnection is the primary candidate for dissipating and converting magnetic energy into relativistic particles and subsequent radiation.

While the initial studies focused on electron-positron plasmas, recent studies have extended into electron-proton plasmas. For high-σ regime ($\sigma \sim \sigma_i \gg 1$), the behavior of reconnection is similar to the pair plasma case and both electrons and protons are efficiently accelerated (Guo et al, 2016b; Zhang et al, 2018). Recent studies have also studied the so-called trans-relativistic regime, where $\sigma_i < 1$ but $\sigma_e \gg 1$, which can lead to strong electron energization (Werner et al, 2018; Ball et al, 2018; Kilian et al, 2020). The transrelativistic regime is also a bridge for connecting the highly relativistic regime ($p \gtrsim 1.5$) with the nonrelativistic reconnection studies ($p \sim 4$) (Dahlin et al, 2014; Li et al, 2021, 2019; Zhang et al, 2021c) (See Oka et al (2023) and Drake et al. in this collection). Traditionally, relativistic magnetic reconnection in the collisionless regime (usually pair plasma) has been less a focus compared to the nonrelativistic cases. The connection between astrophysical reconnection with (non-relativistic) reconnection in other field of research is strong and communications should be continuously encouraged.

In this paper, we review the recent progress in understanding magnetic reconnection in the relativistic magnetically dominated regime. We discuss the astrophysical systems that host magnetic reconnection and how magnetic reconnection may explain high-energy astrophysics observations (Section 1.1). We introduce a list of outstanding problems in relativistic magnetic reconnection in Section 1.2. Section 2 discusses MHD models of relativistic magnetic

reconnection. In Section 3, we discuss the reconnection structure and rate, as well as the generalized Ohm's law. Section 4 discusses the heating and acceleration due to relativistic magnetic reconnection. We will discuss basic acceleration mechanisms, the main features of nonthermal particle acceleration spectra, and the physics that determines the spectra, such as the low-energy injection and energy partition, power-law formation, and high-energy roll-over. Section 5 provides a final remark and possible future directions.

1.1 Where and how magnetic reconnection may happen in astrophysical systems?

Relativistic outflows such as pulsar winds and relativistic jets are launched with energy carried largely in the form of Poynting flux (Coroniti, 1990; Spruit, 2010). However, the magnetic energy in the flows must be eventually converted into energies in thermal and nonthermal particles to power the observed emission signatures. There are ample observational evidence indicating that astrophysical systems with strong magnetic field dissipation support efficient particle acceleration and high-energy radiation (Abdo et al, 2011; Tavani et al, 2011; Abeysekara et al, 2017; Zhang et al, 2015; Ackermann et al, 2016). Magnetic reconnection is a leading mechanism in explaining this underlying process.

Fig. 1 summarizes several systems and environments where magnetic reconnection can be found. In pulsar wind nebulae (PWNe), the antiparallel component of the pulsar dipole field gives rise to a current sheet. The fast rotation of the obliquely oriented dipole leads to the so-called striped wind, where magnetic field directions reverse alternatively and can support magnetic reconnection in the equatorial region. Magnetic reconnection may occur starting from the pulsar magnetosphere (Arons, 2012; Uzdensky and Spitkovsky, 2014; Philippov and Kramer, 2022) to the pulsar wind (Lyubarsky and Kirk, 2001; Kirk and Skjæraasen, 2003), and in the downstream of the termination shock driven by the shock compression (Sironi and Spitkovsky, 2011; Lu et al, 2021). A similar situation can happen in relativistic jets, so-called striped jets (Zhang and Giannios, 2021). For the pulsar wind and pulsar magnetosphere, it is known that close to the neutron star, σ is very high. In fact, how the magnetic field energy is dissipated before pulsar winds reach the termination shock is one of the unsolved science questions in the physics of PWNe ("σ problem"). Magnetic reconnection in the wind and/or at the termination shock is the key process for solving the problem (Coroniti, 1990; Kirk and Skjæraasen, 2003; Sironi and Spitkovsky, 2011; Lu et al, 2021; Zrake, 2016). In the more extreme limit, the magnetic field in magnetars can be strong enough to trigger QED effects (Uzdensky, 2011). Current sheets may develop during neutron star coalescence as their magnetospheres interact, leading to magnetic reconnection (Palenzuela et al, 2013). Magnetic reconnection in highly magnetized regimes of pulsar magnetosphere has been proposed to drive fast ratio bursts (e.g., Philippov et al, 2019).

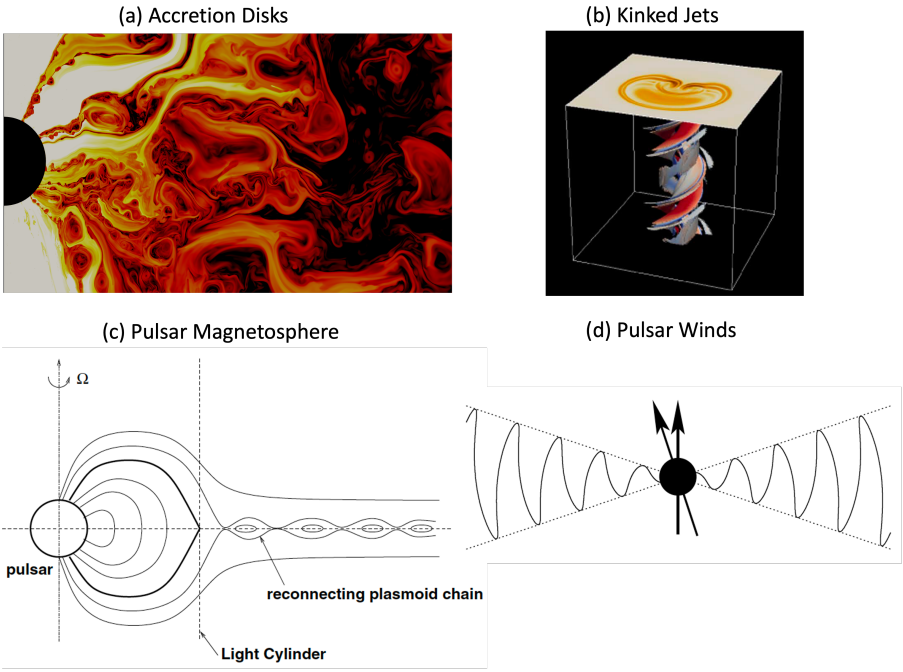

Fig. 1 Several examples of high-energy astrophysical systems that host magnetic reconnection: a) Accretion disks of black holes (Figure created by Bart Ripperda using global GR MHD simulations (Ripperda et al, 2020)), b) Kinked relativistic jets (Zhang et al, 2018), c) pulsar magnetosphere (Uzdensky and Spitkovsky, 2014), and d) pulsar wind nebulae (Kirk and Skjæraasen, 2003). b), c) and d) are reproduced by permission of the AAS.

Close to black holes, magnetic reconnection has also been proposed to explain emissions from accretion disks and relativistic jets. Magnetic reconnection can happen in the accretion disks and their coronae (Hoshino, 2015; Ball et al, 2018; Ripperda et al, 2020; Nathanail et al, 2022; Lin et al, 2023). As kink instability in jets evolves nonlinearly (Zhang et al, 2017; Bodo et al, 2021), it can develop field-line reversals and support magnetic reconnection[2]. In gamma-ray burst models, collisions of relativistic outflows with different magnetic field orientations (Zhang and Yan, 2011). Magnetic reconnection may provide the efficient energy dissipations needed in explaining gamma-ray bursts (Zhang and Yan, 2011; McKinney and Uzdensky, 2012). Magnetic reconnection may explain polarized radiation signatures (Zhang et al, 2018). Recent GR MHD simulations show that magnetic reconnection can happen in the accretion disk. Especially, there exists a low-β corona that may have the right condition for strong particle acceleration and power the nonthermal emission (Ripperda et al, 2020; Yang et al, 2022).

A number of radiation scenarios have been developed to explain high-energy emissions from astrophysical objects. One of the strong motivations to consider

[2]We note that the kink instability itself can also support magnetic energy conversion and particle acceleration (Alves et al, 2018).

magnetic reconnection is the Crab flare, where particles are likely to be accelerated to 10^{15} eV, and it is difficult for a shock model to explain it and avoid synchrotron cooling. Uzdensky and colleagues have proposed that extreme acceleration can happen in the reconnection region with a weak magnetic field ($E > B$) and exceed the "burnoff limit" (Uzdensky et al, 2011; Cerutti et al, 2013). Whether this can be realized is still an active field of research. In particular, whether the global observable effect or only beaming at kinetic scale can be observed is under investigation (Mehlhaff et al, 2020). Reconnection has also been used to explain the high energy emission and fast radiation variability in blazars from black holes as the reconnection outflows can Lorentz boost the radiation (Giannios et al, 2009). However, kinetic simulations observe only small regions/structures close to the upper limit of the Alfvén Lorentz factor, and therefore it is still uncertain if the "minijet model" can actually work (Guo et al, 2015; Sironi et al, 2016). In addition, the condition for obtaining these minijets requires a very weak guide field (Liu et al, 2017). How to achieve these conditions is still unclear and requires further study. Magnetic reconnection may also provide an explanation for time-dependent emissions (Petropoulou et al, 2016) and polarized emissions in blazars (Zhang et al, 2018, 2021c). However, it is unclear if these radiation features are still preserved in 3D reconnection, where the flux ropes are shown to be highly dynamical and can easily be disrupted (Guo et al, 2021, 2016a).

It is also interesting to mention that magnetic reconnection can happen in the foreshock region for high Mach number shocks (Matsumoto et al, 2015). Several numerical simulations have indicated that a number of current sheets can be generated by the ion Weibel instability during the interaction of incoming and reflected ions at the foreshock region (Kato and Takabe, 2008; Spitkovsky, 2008; Burgess et al, 2016), and it is suggested that magnetic reconnection may play an important role on electron heating and acceleration as the so-called shock injection process into the first-order Fermi acceleration (Bohdan et al, 2020).

1.2 Key Physics Issues

Before getting into the detailed discussion, we close this section by discussing a list of frontier physical problems that is currently undergoing active studies in relativistic magnetic reconnection.

The *Rate Problem* (see Sections 2 and 3) is one of the long-standing problems in magnetic reconnection and is concerned with how fast magnetic reconnection proceeds. While the original Sweet-Parker model cannot support fast reconnection, recent MHD and kinetic theories have shown the rate can be $R \sim 0.01 - 0.3$. Figuring out how fast magnetic energy is dissipated helps explain astrophysical magnetic energy release. Learning the reconnecting electric field helps us to understand the upper limit of particle acceleration that magnetic reconnection can explain.

The *Particle Heating and Acceleration Problem* (Section 4) is to understand how magnetic energy is converted and partitioned into thermal and

nonthermal particles, and how a population of particles are accelerated to high energy. An important goal of the particle energization problem is to build a complete understanding of the physics processes involved and predict the resulting distributions of energetic particles during relativistic magnetic reconnection. Competing theories have been proposed based on various reconnection models, but there is still no general consensus on the origin of nonthermal distributions observed during magnetic reconnection.

The Onset Problem: Most studies have been focusing on pre-existing current sheets. However, the current sheet needs to form at the first place, which is a dynamical and sometimes prolonged process (e.g., Uzdensky and Loureiro, 2016; Tenerani et al, 2016; Huang et al, 2017; Comisso et al, 2017). In addition, how magnetic energy is accumulated and stored prior to the onset is unknown. Thus it is important to include the formation of current sheets and its effect. In addition, learning how reconnection onsets help understand the conditions that lead to explosive energy release in astrophysics.

Multiscale Problem and reconnection in global models: Reconnection in most astrophysical problems must involves both MHD scales and kinetic scales. While MHD models offer a basic description of large-scale magnetic reconnection, studies have shown kinetic effects are essential. Developing a self-consistent treatment that including multi-scale effects is of central importance. In addition, developing global particle acceleration models is essential for describing particle acceleration in realistic systems and connecting with observations.

3D Reconnection and Effects of Turbulence: The main issue here is to understand how reconnection properties and associated particle acceleration change compared to 2D reconnection. A closely related problem is the role of turbulence, either externally driven or self-generated during the reconnection process. Recently, 3D kinetic simulations and high-Lundquist-number MHD simulations (with and without preexisting turbulence) have been carried out. However, it is still unclear if and how the reconnection physics strongly influence by turbulence. Meanwhile, there seems to be promising evidence suggesting that particle acceleration in 3D becomes substantially different. We will discuss the 3D effects and role of turbulence in the following sections as we discuss individual topics.

The *Radiation Problem* is to study the effect of radiation cooling (on reconnection structure), pair production, radiation pressure, etc. In addition, there are strong interests in modeling the radiation signature to explain observations. This is not the focus of this review but we refer interested readers to the recent papers by Jaroschek and Hoshino (2009); Uzdensky (2011).

2 Fluid Simulations of Relativistic Reconnection

2.1 Early theories

Blackman and Field (1994) presented the first theoretical models of steady reconnection. By constructing relativistic Sweet–Parker and Petschek models, they pointed out that plasma density in the outflow region increases due to Lorentz contraction. Since this in turn requires relativistically fast plasma inflow, they claimed that the reconnection rate can be relativistic. Lyutikov and Uzdensky (2003) further examined relativistic Sweet–Parker model and suggested that reconnection outflow speed may exceed inflow Alfven speed. Later, Lyubarsky (2005) have developed theoretial models of relativistic Sweet–Parker and Petschek reconnection, taking compressibility into account. In the relativistic regime, he pointed out that the internal energy density in the outflow region is high enough to increase the effective plasma inertia. For this reason, he claimed that the reconnection outflow is only mildly relativistic. In addition, considering full momentum balance in Petschek model, he predicted that the opening angle of slow shocks will be smaller. This leads Lyubarsky to argue that the reconnection remains "slow" ($\sim \mathcal{O}(0.1)$), because it is difficult to transport energy through a narrow outflow exhaust.

2.2 Basic equations

To validate the theories, several numerical models have been developed, however, basic equations need to be developed. Roughly speaking, two numerical models have been used, the relativistic resistive magnetohydrodynamics (RRMHD) and relativistic multifluid dynamics.

The RRMHD model was first developed by Watanabe and Yokoyama (2006). Combining relativistic fluid equations, Ohm's law, and Maxwell equations, they have organized the following set of RRMHD equations,

$$\partial_t(\Gamma\rho) + \nabla\cdot(\rho\mathbf{U}) = 0, \tag{2}$$

$$\partial_t(\Gamma w\mathbf{U} + \mathbf{E}\times\mathbf{B}) + \nabla\cdot\left((P + \frac{B^2+E^2}{2})\mathbb{I} + w\mathbf{U}\mathbf{U} - \mathbf{B}\mathbf{B} - \mathbf{E}\mathbf{E}\right) = 0, \tag{3}$$

$$\partial_t(\Gamma^2 w - P + \frac{B^2+E^2}{2}) + \nabla\cdot(\Gamma w\mathbf{U} + \mathbf{E}\times\mathbf{B}) = 0, \tag{4}$$

$$\partial_t\mathbf{B} + \nabla\times\mathbf{E} = 0, \qquad \partial_t\mathbf{E} - \nabla\times\mathbf{B} = -\mathbf{J}, \tag{5}$$

$$\partial_t\rho_c + \nabla\cdot\mathbf{J} = 0, \tag{6}$$

$$\Gamma\left(\mathbf{E} + \mathbf{V}\times\mathbf{B} - (\mathbf{E}\cdot\mathbf{V})\mathbf{V}\right) = \eta(\mathbf{J} - \rho_c\mathbf{V}) \tag{7}$$

Here, we have used Lorentz–Heaviside notations with $c = 1$. In equations, $\Gamma \equiv 1/\sqrt{1-(V/c)^2}$ is the Lorentz factor, ρ is the proper density, $\mathbf{U} = \Gamma\mathbf{V}$ is the 4-vector, w is the relativistic enthalpy, P is the proper pressure, $\mathbb{I}$ is

the identity matrix, and ρ_c is the charge density. The internal energy in the relativistic enthalpy is often approximated by a simple equation of state with the adiabatic index $\Gamma_a = 4/3$. In such a case, the enthalpy is given by $w = \rho c^2 + [\Gamma_a/(\Gamma_a - 1)]P$. Eq. (7) relates the electric field and the electric current density in the $\mathbf{V}$-moving frame with a coefficient η.

Practically, Eqs. (5) are often replaced by the following equations (Komissarov, 2007).

$$\partial_t \mathbf{B} + \nabla \times \mathbf{E} + \nabla \Phi = 0, \qquad \partial_t \mathbf{E} - \nabla \times \mathbf{B} + \nabla \Psi = -\mathbf{J}, \tag{8}$$

$$\partial_t \Phi + \nabla \cdot \mathbf{B} = -\kappa \Phi, \qquad \partial_t \Psi + \nabla \cdot \mathbf{E} = \rho_c - \kappa \Psi, \tag{9}$$

Here, Φ, Ψ, κ are virtual potentials and the decay coefficient in order to reduce numerical errors in $\nabla \cdot \mathbf{B}$ and $\nabla \cdot \mathbf{E}$ by the so-called hyperbolic divergence cleaning method (Munz et al, 2000; Dedner et al, 2002). In the RRMHD equations, the electric field is known to be very stiff, when the resistivity η is low. To deal with these issues, various schemes have been developed such as the operator splitting (Komissarov, 2007), implicit schemes (Palenzuela et al, 2009; Dumbser and Zanotti, 2009; Mignone et al, 2019), and a method of characteristics (Takamoto and Inoue, 2011). Other extensions include the Galerkin method (Dumbser and Zanotti, 2009) and generalized equation of states (EoSs) (Mizuno, 2013).

Another approach is to use relativistic multifluid equations. Zenitani et al (2009a,b) have proposed the following relativistic multifluid equation systems. For electron-positron two-fluid plasma, this equation system is also known as relativistic two-fluid electrodynamics. They consist of relativistic fluid equations and Maxwell equations.

$$\partial_t(\Gamma_p n_p) = -\nabla \cdot (n_p \mathbf{U}_p), \tag{10}$$

$$\partial_t\Big(\Gamma_p w_p \mathbf{U}_p\Big) = -\nabla \cdot \Big(w_p \mathbf{U}_p \mathbf{U}_p + P_p \mathbb{I}\Big) + \Gamma_p n_p q_p (\mathbf{E} + \mathbf{V}_p \times \mathbf{B}) - \tau n_p n_e (\mathbf{U}_p - \mathbf{U}_e), \tag{11}$$

$$\partial_t\Big(\Gamma_p^2 w_p - P_p\Big) = -\nabla \cdot (\Gamma_p w_p \mathbf{U}_p) + \Gamma_p n_p q_p (\mathbf{V}_p \cdot \mathbf{E}) - \tau n_p n_e (\Gamma_p - \Gamma_e), \tag{12}$$

$$\partial_t(\Gamma_e n_e) = -\nabla \cdot (n_e \mathbf{U}_e), \tag{13}$$

$$\partial_t\Big(\Gamma_e w_e \mathbf{U}_e\Big) = -\nabla \cdot \Big(w_e \mathbf{U}_e \mathbf{U}_e + P_e \mathbb{I}\Big) + \Gamma_e n_e q_e (\mathbf{E} + \mathbf{V}_e \times \mathbf{B}) - \tau n_p n_e (\mathbf{U}_e - \mathbf{U}_p), \tag{14}$$

$$\partial_t\Big(\Gamma_e^2 w_e - P_e\Big) = -\nabla \cdot (\Gamma_e w_e \mathbf{U}_e) + \Gamma_e n_e q_e (\mathbf{V}_e \cdot \mathbf{E}) - \tau n_p n_e (\Gamma_e - \Gamma_p), \tag{15}$$

$$\partial_t \mathbf{B} = -\nabla \times \mathbf{E}, \qquad \partial_t \mathbf{E} = \nabla \times \mathbf{B} - 4\pi (q_p n_p \mathbf{U}_p + q_e n_e \mathbf{U}_e). \tag{16}$$

In these equations, the subscript p indicates positron properties (and e for electrons), n is the proper number density, τ is a friction coefficient. For simplicity, the rest mass m and the light speed c are set to 1. Note that interspecies friction terms are added to the right-hand sides of the momentum and energy equations (Zenitani et al, 2009b). From MHD viewpoint, an effective resistivity stems from the friction term and the fluid inertial terms.

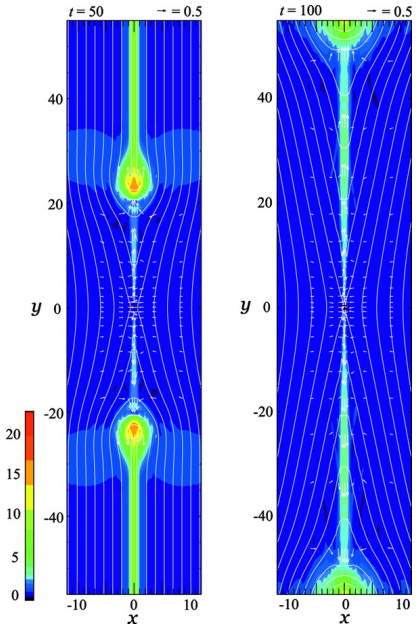

Fig. 2 Evolution of plasma density from RRMHD simulation with $\sigma = 4.0$ and localized resistivity. The solid lines and the arrows show magnetic field lines and velocity vectors. [Adapted from Watanabe and Yokoyama (2006), reproduced by permission of the AAS]

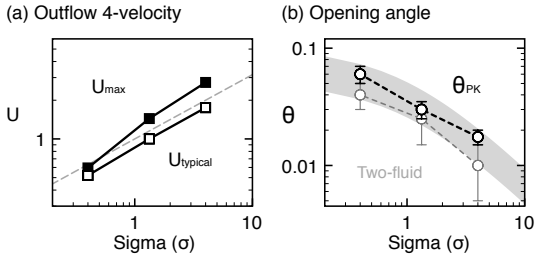

Fig. 3 (a) Maximum and typical 4-velocities U_x as a function of the inflow σ. The dashed line indicates an Alfvén speed in Eq. (17). (b) Opening angles of the Petschek slow shocks in RRMHD (black line) and in two-fluid (gray) simulations. The shadow indicates a predicted scaling of $\propto (1+\sigma)^{-1}$. [Adapted from Zenitani et al (2010), reproduced by permission of the AAS]

Similarly, divergence cleaning potentials are often used to improve the numerical accuracy (Eqs. (8) and (9)). Numerical schemes to better solve these equations have been actively developed over years (Barkov et al, 2014; Balsara et al, 2016; Amano, 2016).

2.3 Relativistic Petschek reconnection

Using RRMHD equations, Watanabe and Yokoyama (2006) have pioneered the MHD-scale evolution of relativistic magnetic reconnection. They have assumed

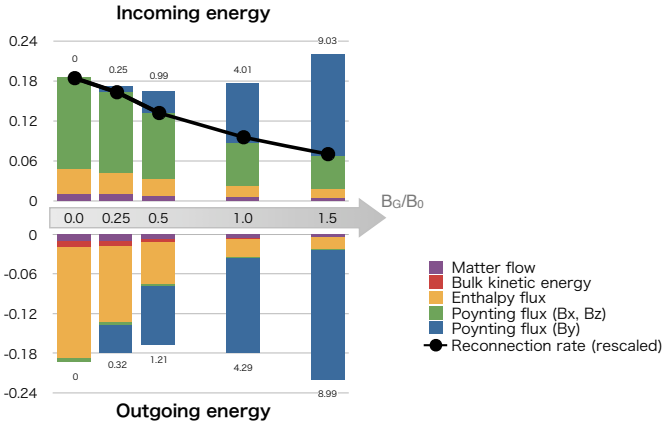

Fig. 4 The incoming and outgoing energy fluxes around the reconnection region. The guide field Poynting flux (B_y), the rest part of Poynting flux (B_x, B_z), the plasma enthalpy flux, the bulk kinetic energy, and the matter flow are presented. The black curve indicates a rescaled reconnection rate. [Adapted from Zenitani et al (2009b), reproduced by permission of the AAS]

a spatially localized resistivity $\eta = \eta(x, z)$ in the relativistic Ohm's law (Eq. 7), and then they have obtained a well-developed picture of relativistic Petschek reconnection. As shown in Fig. 2, a narrow reconnection jet extends from the central reconnection point. The reconnection jet is surrounded by a pair of slow shocks, similar to nonrelativistic Petschek reconnection (Petschek, 1964). It appears that the outflow channel is much narrower than in the nonrelativistic case. These features were further examined by subsequent studies by two-fluid (Zenitani et al, 2009a,b) and the RRMHD simulations (Zenitani et al, 2010; Zanotti and Dumbser, 2011).

It has been found that the typical outflow speed is approximated by the upstream Alfvén speed (Zenitani et al, 2010),

$$V_{\rm out} \approx c_{\rm A,up} = [\sigma/(1+\sigma)]^{1/2}, \tag{17}$$

where $\sigma \equiv B^2/w$ (in the Lorentz–Heaviside units) is the magnetization parameter in the upstream region. This relation in the 4-velocity form is indicated by the white squares in Fig. 3(a). Also, the opening angle of the Petschek outflow becomes narrower and narrower as the system becomes relativistic, as confirmed in Fig. 3(b). These results are in excellent agreement with theoretical predictions by Lyubarsky (2005). Numerical simulations have revealed that the reconnection rate is $\mathcal{R} = \mathcal{O}(0.1)$ or even faster. Theoretically, such a fast reconnection was questioned before, because the outflow channel may be too narrow to eject a sufficient amount of energy from the reconnection region (Lyubarsky, 2005). Based on the numerical results in the relativistic two-fluid model (Zenitani et al, 2009b), we explain this logical gap in the following way.

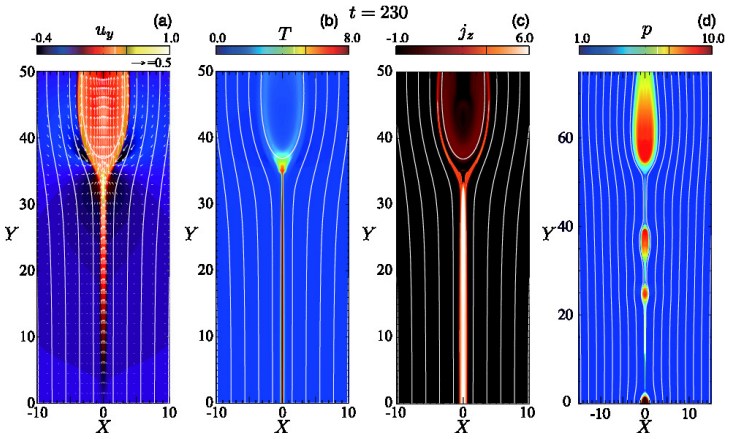

Fig. 5 Sweet–Parker results from RRMHD simulations with uniform resistivity. (a) The outflow component of the four velocity (U_y), (b) the plasma temperature ($T = P/\rho$), and (c) the out-of-plane electric current density (J_z) are presented. The Lundquist number is $S \sim 10^{3.5}$. (d) The plasma pressure (P) with $S \sim 10^4$. The solid lines show the magnetic field lines. [Adapted from Takahashi et al (2011), reproduced by permission of the AAS]

Fig. 4 presents the composition of the incoming and outgoing energy flow during the quasi-steady stage of reconnection. In the antiparallel (leftmost) case with $B_{\rm G} = 0$, it has been found that the energy is mostly carried away in the form of the relativistic enthalpy flux, $\sim \sum_{i=p,e} 4\Gamma^2 P\mathbf{V}$, which was often overlooked by the earlier theories. In other words, since the enthalpy flux can carry a huge amount of energy per unit rest mass, it allows fast reconnection even through the narrow outflow channel.

2.4 Relativistic Sweet–Parker reconnection

Takahashi et al (2011) have studied basic properties of Sweet–Parker reconnection. They employed a uniform resistivity in the Ohm's law (Eq. 7), and then they have examined an RRMHD evolution of Sweet–Parker reconnection. A laminar Sweet–Parker current sheet was successfully reproduced in Figs. 5a–c. By changing the Lundquist number S ($\propto \eta^{-1}$) from 2×10^3 to 2×10^4, they have confirmed that the reconnection rate scales like $\propto S^{-1/2}$, as predicted by the relativistic Sweet–Parker theory (Lyubarsky, 2005). It was also reported that the outflow speed is sub-Alfvénic, because of the larger inertia by the relativistic enthalpy.

Similar to the nonrelativistic MHD reconnection, when the Lundquist number exceeds $S \gtrsim \mathcal{O}(10^4)$, the Sweet–Parker current sheet becomes turbulent, because of the repeated formation of plasmoids (Biskamp, 1986; Loureiro et al, 2007; Bhattacharjee et al, 2009; Uzdensky et al, 2010). An early signature of the plasmoid-dominated regime can be seen in Fig. 5d, but an RRMHD version of plasmoid-dominated turbulent reconnection has been studied by Takamoto (2013). Fig. 6(a) shows a representative result for $S \sim 10^{5.5}$. One can see plasmoids with various sizes. Fig. 6(b) presents the S-dependence of

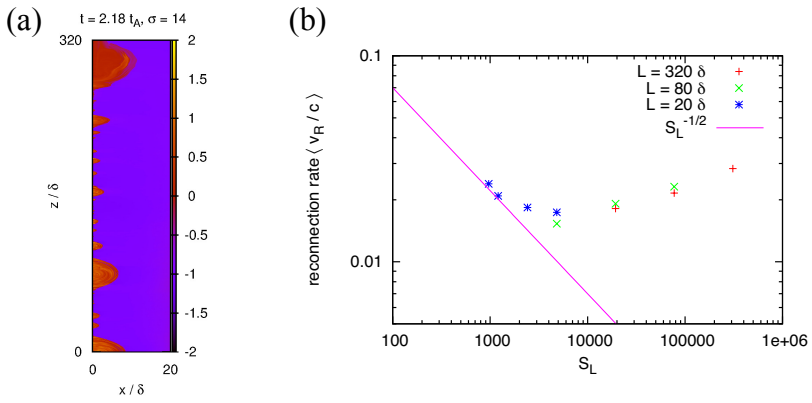

Fig. 6 (a) Plasma temperature T/mc^2 from an RRMHD simulation with $S \sim 10^{5.5}$ and $\sigma = 14$. (b) Time-averaged reconnection rate in the $\sigma = 14$ runs, as a function of the Lundquist number S. [Adapted from Takamoto (2013), reproduced by permission of the AAS].

the reconnection rate. The magenta line indicates the rate by the relativistic Sweet–Parker theory, which was numerically verified by Takahashi et al (2011). For higher-S regime of $S \gtrsim \mathcal{O}(10^4)$, the system becomes plasmoid-dominated the reconnection system becomes plasmoid-dominated. As a result, the reconnection rate deviates from the Sweet–Parker rate, and it remains fast $\sim \mathcal{O}(0.01)$ regardless of S.

2.5 Dependence to the resistivity model

Similar to the nonrelativistic case, the system evolution is sensitive to the effective resistivity model. Relativistic Petschek reconnection evolves under a spatially-localized resistivity in the RRMHD and relativistic two-fluid models (Watanabe and Yokoyama, 2006; Zenitani et al, 2009a, 2010; Zanotti and Dumbser, 2011). In the RRMHD model, Sweet-Parker (Takahashi et al, 2011) and plasmoid-dominated turbulent reconnections (Takamoto, 2013) evolve under a spatially uniform resistivity. Meanwhile, when we employ a uniform friction parameter (τ) in the relativistic two-fluid model, multiple plasmoids appear in the reconnecting current sheet, as shown in Fig. 7. This differs from the RRMHD results, because the resistivity model is no longer the same. In the relativistic two-fluid model, the fluid inertia terms also play a role similar to a resistivity. Finally, under a current-dependent resistivity, repeated-formation of plasmoids are observed in the RRMHD model (Zenitani et al, 2010). For practical applications of the RRMHD model, a good form of parameter-dependent resistivity needs to be developed.

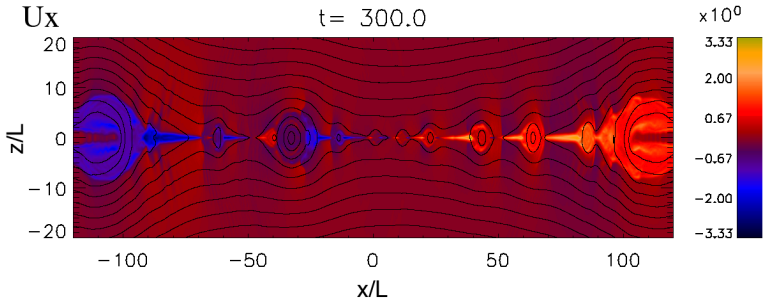

Fig. 7 The x-component of the plasma 4-velocity $U_x = (\Gamma V)_x$ from a relativistic two-fluid simulation with uniform resistivity. The black lines show magnetic field lines. [Adapted from Zenitani et al (2009a), reproduced by permission of the AAS].

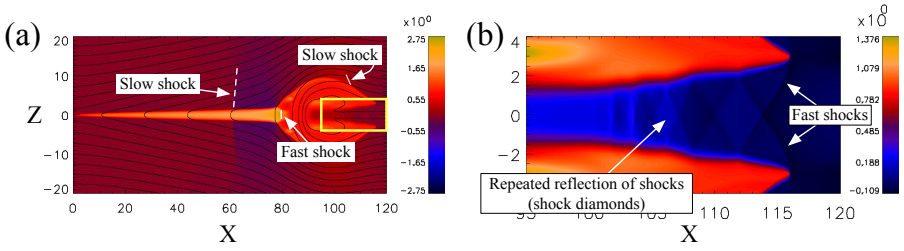

Fig. 8 (a) A spatial profile of the x-component of the plasma 4-velocity $U_x = (\Gamma V)_x$ from an RRMHD simulation with localized resistivity. The black lines show magnetic field lines. (b) A profile of U_x in the front side of the plasmoid, $x \in [95, 120]$ and $z \in [-4, 4]$ (corresponding to the yellow box in panel (a)). [Modified from Zenitani et al (2010), reproduced by permission of the AAS].

2.6 Shocks in the reconnection system

We discuss another feature of relativistic magnetic reconnection in the fluid regime — the system is often dominated by shocks. We remind the readers that the relativistic sound speed is slower than $1/\sqrt{3}$ ($c/\sqrt{3}$). In contrast, the outflow speed can be faster and faster (Eq. (17)), as the magnetization σ increases in the upstream region. Comparing these relations, we find that the outflow jet always becomes supersonic when $\sigma > 1/2$. In such a supersonic regime, the outflow jets and the outflow-driven plasmoids generate shocks.

In single-reconnection systems, Zenitani et al (2010) have reported various shocks around the plasmoid ahead of the reconnection jet, as indicated in Figs. 8(a) and (b). These shocks are essentially attributed to supersonic or transonic reconnection jet, but they need to be studied in further detail. Even though Takamoto (2013) has explored other important aspects, no one has explored shocks in plasmoid-dominated systems. We expect that the plasmoid-dominated turbulent reconnection is also shock-dominated in high-σ regimes, as potential signatures can be seen in vertical discontinuities Fig. 7. To numerically deal with these shocks, we need to use shock-capturing simulation codes.

Most of recent codes are capable of shocks by using HLL-type upwind schemes (Komissarov, 2007; Palenzuela et al, 2009; Mizuno, 2013; Mignone et al, 2019).

2.7 Discussion

These simulations have revealed fluid-scale properties of relativistic magnetic reconnection. Relativistic MHD reconnections are basically similar to nonrelativistic MHD reconnections – relativistic Petschek (Watanabe and Yokoyama, 2006; Zenitani et al, 2009a, 2010), relativistic Sweet–Parker (Takahashi et al, 2011), and relativistic plasmoid-mediated reconnections (Takamoto, 2013) are reported. The resistivity model determines the system evolution, as discussed in Section 2.5. In these regimes, the system can be dominated by shocks. At this point, the number of RRMHD reconnection studies is still limited. Many issues, such as influence of the environmental parameters, remain unsolved. For example, dependence to magnetization parameters: $\sigma \equiv B^2/w$ or $\sigma_m \equiv B^2/\rho$ guide-field, flow-shear, and asymmetry needs to be explored.

Beyond the special relativity, several groups have been actively developing advanced Runge-Kutta codes for general relativistic resistive MHD (GR-RMHD) (Bucciantini and Del Zanna, 2013; Dionysopoulou et al, 2013; Ripperda et al, 2019). Inda-Koide et al (2019) have also developed an HLL-type GR-RMHD code to study magnetic reconnection close to the black hole. These GR-RMHD codes are successfully used to study the black hole and its accretion disk systems, however, influence of GR effects to the local reconnection physics remain unclear. Combining radiative transfer equations with the RRMHD equations, Takahashi and Ohsuga (2013) have developed a relativistic radiative resistive MHD (RRRMHD) model. Numerical results of RRRMHD reconnections look similar to the conventional RRMHD results, however, the number of works are quite limited. There are strong demand for further studies, to understand GR and/or radiation effects to RRMHD reconnection.

3 Relativistic Reconnection in Collisionless Plasmas

While MHD simulations provide decent descriptions of reconnection process over large scales, the diffusion region is likely collisionless in many active regions of interest. Two-fluid simulations describe part of the kinetic physics, but Particle-in-Cell (PIC) simulations can capture the full kinetics. Hence, in this section, we report the up-to-date progress in understanding relativistic reconnection using PIC simulations, which reveal the kinetic physics that breaks the ideal condition and the key to fast magnetic reconnection in astrophysical collisionless plasmas.

3.1 Relativistic Generalized Ohm's Law

During magnetic reconnection, magnetic flux is transported across the X-line. This requires the violation of the ideal condition $\mathbf{E}+(\mathbf{V}/c)\times\mathbf{B} = 0$, where $\mathbf{V}$ is

the bulk plasma velocity. Understanding the physical mechanism that breaks the ideal condition is one of the most important topics in reconnection physics, and the generalized Ohm's law is critical in determining such a mechanism, as also discussed in the non-relativistic limit (Liu et al. 2023, this issue).

The extension of the generalized Ohm's law can be nontrivial, and different formalism was derived from the electron momentum equation (Hesse and Zenitani, 2007; Zenitani, 2018). Here we discuss the latest form derived in Zenitani (2018). For simplicity, the speed of light is set to be $c = 1$. We begin with the stress-energy tensor

$$T^{\alpha\beta} = \int f(u) u^\alpha u^\beta \frac{d^3u}{\gamma}. \tag{18}$$

where $u^\alpha = (\gamma, \gamma\mathbf{v})$ is the particle four-velocity and particle Lorentz factor $\gamma = 1/\sqrt{1-(v/c)^2}$. A Greek index (e.g., α, β) runs from 0 to 3 to account for four-dimensional spacetime. Using a four-velocity of the bulk flow $U^\alpha = (\Gamma, \Gamma\mathbf{V})$ where the fluid Lorentz factor $\Gamma = 1/\sqrt{1-(V/c)^2}$, the metric tensor $g^{\alpha\beta} = \mathrm{diag}(-1,1,1,1)$, and the projection operator $\Delta^{\alpha\beta} = g^{\alpha\beta} + U^\alpha U^\beta$, the stress-energy tensor can be decomposed into (Eckart, 1940):

$$T^{\alpha\beta} = \mathcal{E} U^\alpha U^\beta + q^\alpha U^\beta + q^\beta U^\alpha + P^{\alpha\beta} \tag{19}$$

Here, $\mathcal{E} \equiv T^{\alpha\beta} U_\alpha U_\beta$ is the invariant energy density, $q^\alpha \equiv -\Delta^\alpha_\beta T^{\beta\gamma} U_\gamma$ is the energy flux (heat flow), and $P^{\alpha\beta} \equiv \Delta^\alpha_\gamma \Delta^\beta_\delta T^{\gamma\delta}$ is the pressure tensor. The momentum part of Eq. (19) is reduced to a familiar combination of the dynamic pressure and the pressure tensor, $T^{ij} = mnV^iV^j + P^{ij}$, in the non-relativistic limit, where a Roman index (e.g., i, j) runs from 1 to 3 to account for the three-dimensional space.

Note that the choice of U^α in Eq. (19) is arbitrary, and several reasonable choices can be considered (See Zenitani (2018) for more detail). Among these choices, here we employ the average plasma velocity $\mathbf{V}$ that carries the electric charge, and it thus satisfies the relation of $J_{\beta,(e)} = -en' U_{\beta,(e)}$, as usual. Here e is the unit charge, n' is the proper number density, and $J_{\beta,(e)}$ is the electric current carried by electrons. We use the prime to denote the proper quantities.

We then use the energy-momentum equation of electrons,

$$\partial_\beta T^{\alpha\beta}_{(e)} = F^{\alpha\beta} J_{\beta,(e)} = -en' F^{\alpha\beta} U_{\beta,(e)} \tag{20}$$

where $F^{\alpha\beta}$ the electromagnetic tensor. Subscript (e) indicates electron fluid properties. However, for brevity, we omit this subscript hereafter in this subsection.

From the spatial parts (i.e., $\beta = 1, 2, 3$) of Eqs. (19) and (20), we obtain the electron Ohm's law,

$$\mathbf{E} = -\mathbf{V} \times \mathbf{B} - \frac{1}{\Gamma en'} \Big[\partial_t T^{i0} + \partial_j (\mathcal{E} U^i U^j + Q^{ij} + P^{ij}) \Big]. \tag{21}$$

where $\mathbf{V}$ is the bulk velocity and $Q^{\alpha\beta} \equiv q^{\alpha}U^{\beta} + q^{\beta}U^{\alpha}$ is the heat-flow part of the stress-energy tensor. The relativistic effects appear in Γ, $\mathcal{E}$ ($> n'mc^2$), Q, and their time derivatives.

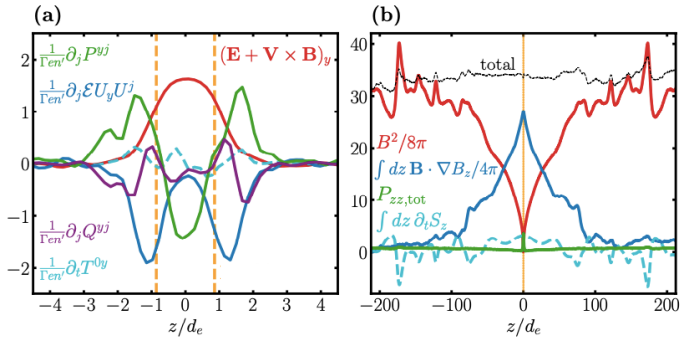

Fig. 9 (a) relativistic Ohm's law (Eq. 21). Each term is color-coded. (b) the force balance along the inflow direction. The yellow vertical dashed lines in (a) and (b) mark the predicted diffusion region edges. [Adapted from Goodbred and Liu (2022)]

Fig. 9 displays the y-component (out of the reconnection plane) of the generalized Ohm's law (for electrons), across the X-line in relativistic magnetic reconnection. One key feature is the dominance of the inertial-like term $\partial_j(\mathcal{E}U_yU^j)$ in blue at the edge of the diffusion region where $[\mathbf{E}+\mathbf{V}\times\mathbf{B}]_y$ in red is finite. This fact can be used to show that the diffusion region thickness is on the electron inertial scale (Goodbred and Liu, 2022), as marked by the yellow dashed vertical lines in Fig. 9(a). This important spatial scale will be used to derive the first-principles reconnection rate in Section 3.2.2. The purple curve indicates the "heat-flow inertial" term, which corresponds to the momentum transport by the energetic electrons that carry the heat flow in the rest frame of electrons (Zenitani, 2018). Relations between the kinetic physics and the terms in Eq. (21) are largely unknown and require more study, because these equations were formulated relatively recently.

The Eckart decomposition is also useful for evaluating the energy balance. The $0i$ components of the plasma stress-energy tensor in Eq. (19) can be further decomposed into the matter flow, the bulk kinetic energy flux, the enthalpy flux, and the heat flux, as respectively shown in the right-hand side of the following equation,

$$T^{0i} = n'U^i + (\Gamma-1)n'U^i + \Big[(\mathcal{E}-n')\Gamma U^i + P^{0i}\Big] + Q^{0i}. \tag{22}$$

Zenitani (2018) reported that most incoming electromagnetic energy is converted into the relativistic enthalpy flux in the downstream region during relativistic magnetic reconnection, in agreement with RRMHD discussion in Section 2.2.

3.2 Relativistic Collisionless Reconnection Rate

Following the presentation laid out in Liu et al., (2023, this issue), we divide the rate problem into a subsection to model the maximum plausible rate and a subsection to discuss the key localization mechanism. In the end, one can derive the reconnection rate as a function of σ_0 from first principles.

3.2.1 *R-S*$_{lope}$ relation and the maximum plausible rate

In strongly magnetized plasmas, the plasma flow speed can be relativistic. During anti-parallel reconnection, the relevant force balance can be described by

$$\frac{\mathbf{B}\cdot\nabla\mathbf{B}}{4\pi} \simeq \frac{\nabla B^2}{8\pi} + \nabla\cdot\mathbf{P} + n' m_i \mathbf{U}\cdot\nabla\mathbf{U}, \tag{23}$$

where $\mathbf{U} = \Gamma\mathbf{V}$, $\Gamma \equiv [1-(V/c)^2]^{-1/2}$ is the Lorentz factor of the bulk flow, and primed quantities are the proper quantities. Balancing the magnetic tension with the plasma inertia along the outflow direction, the resulting outflow speed is the relativistic Alfvén speed

$$V_{A0} = c\sqrt{\frac{\sigma_{x0}}{1+\sigma_{x0}}}. \tag{24}$$

which is limited by the speed of light when the cold magnetization parameter $\sigma_{x0} = B_{x0}^2/4\pi n' mc^2 \gg 1$. Here B_{x0} is the asymptotic value of the reconnecting magnetic field component.

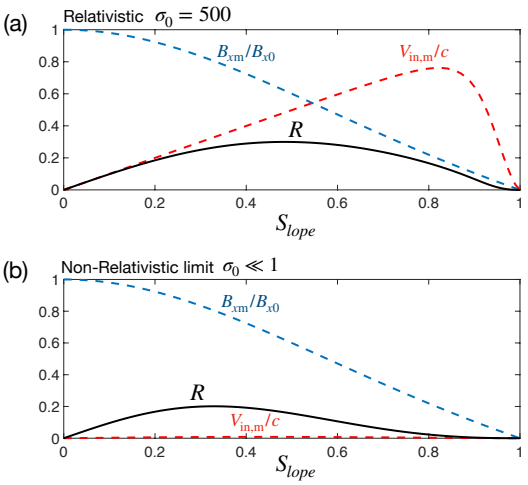

Fig. 10 The $R - S_{lope}$ relation. (a) predicted reconnection rate R, microscale inflow speed $V_{in,m}/c \simeq E_y/B_{xm}$, and field reduction B_{xm}/B_{x0} as a function of separatrix S_{lope} in the relativistic regime; (b) predictions in the non-relativistic limit [Modified from Liu et al (2017)]

However, when the outflow geometry opens out, we need to consider the difference at the microscale (denoted by subscript "m") and the mesoscale at the asymptotic region (denoted by subscript "0"). Following the same approach laid out in Liu et al. (2023, this issue), analyzing the force balance along the inflow (e.g., Fig. 9(b)) and retaining the magnetic pressure ($\nabla B^2/8\pi$), Liu et al (2017) derived

$$\frac{B_{xm}}{B_{x0}} \approx \frac{1-S_{lope}^2}{1+S_{lope}^2}. \tag{25}$$

where S_{lope} is the slope of the separatrix. Similarly, analyzing the force balance along the outflow, retaining the magnetic pressure ($\nabla B^2/8\pi$), one can derive the outflow speed at the downstream boundary of the diffusion region

$$V_{out,m} \simeq c\sqrt{\frac{(1-S_{lope}^2)\sigma_{xm}}{1+(1-S_{lope}^2)\sigma_{xm}}}. \tag{26}$$

The reconnection rate, by definition, is

$$R \equiv \frac{cE_y}{B_{x0}V_{A0}} = \left(\frac{B_{zm}}{B_{xm}}\right)\left(\frac{B_{xm}}{B_{x0}}\right)\left(\frac{V_{out,m}}{V_{A0}}\right), \tag{27}$$

which can be derived through plugging in Eqs. (25), (26), (24), and realizing that $B_{zm}/B_{xm} \simeq S_{lope}$.

As the separatrix slope increases, the B_{xm}/B_{x0} ratio decreases. Simulation suggests that in the high-σ limit, the B_{xm}/B_{x0} ratio can be significantly lower than that in the non-relativistic limit, which leads to a much higher microscopic inflow speed $V_{in,m}$ at the upstream boundary of the diffusion region, as predicted in Fig. 10(a). In spite of this relativistic inflow speed ($\sim 0.8c$), a value around 0.3 still upper bounds the relativistic reconnection rate R. In comparison, the maximum plausible rate in the non-relativistic limit (Fig. 10(b)) is around 0.2, where the microscopic inflow speed is much lower than the speed of light.

3.2.2 Localization mechanism that leads to fast reconnection

In electron-positron (pair) plasmas, the Hall effect [Liu et al (2022), also discussed in Liu et al. (2023, this issue)] is absent, but the pressure depletion appears to be significant. This is evident in Fig. 11, which shows the positron pressure P_{izz} contour in the top panel and its cut along the outflow symmetry line in the middle panel. The initial positron (also electron) pressure that can balance the asymptotic magnetic pressure is marked by the red dashed horizontal line of value 100 in the middle panel, while the P_{izz} cut at this nonlinear stage indicates a much lower value at the X-line. (p.s., those peaks are secondary plasmoids that will be discussed later). We can show that the relativistic Lorentz factor associated with the large electric current density is responsible for this drastic pressure depletion, which leads to fast reconnection in ultra-relativistic astrophysical plasmas.

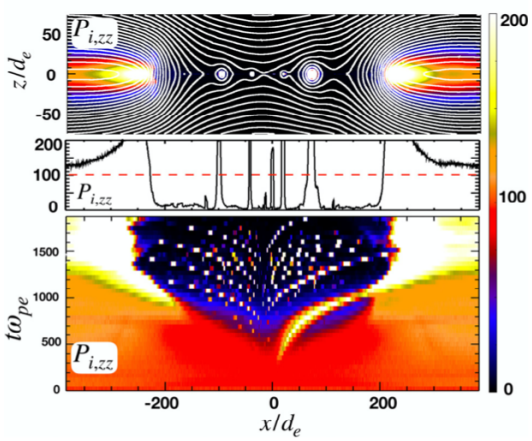

Fig. 11 The pressure depletion and bursty nature of relativistic reconnection with $\sigma_{x0} \simeq 89$. The P_{izz} contour in the top panel, P_{izz} cut along $z = 0$ in the middle panel, and the time stack plot in the bottom panel. The red dashed horizontal line in the middle panel marks the initial plasma pressure. [Adapted from Liu et al (2020), reproduced by permission of the AAS]

Goodbred and Liu (2022) managed to model this effect analytically. By considering the energy conservation along the narrow inflow channel toward the X-line, they derived the upper bound value of the X-line pressure,

$$P_{zz}|_{xline} \leq 2n'_{xline}mc^2 \left[\frac{\langle \gamma(v_z) \rangle_{xline}}{\Gamma_y} - \frac{\Gamma_y}{\langle \gamma(v_z) \rangle_{xline}} \right]. \tag{28}$$

This expression (Eq. (28)) makes clear the factors affecting the x-line thermal pressure. While $\langle \gamma(v_z) \rangle_{xline}$ is controlled by the energy per particle that also includes thermal motions in v_z, Γ_y is purely controlled by the bulk flow of current carriers that drift in the y-direction. If all available energy is used to drive the current, then $\Gamma_y \simeq \langle \gamma(v_z) \rangle_{xline}$, and $P_{zz}|_{xline}$ becomes very small. Conversely, if only a small fraction of the total energy is needed to drive the current, $P_{zz}|_{xline}$ can become significant. The predicted x-line pressure normalized to the asymptotic magnetic pressure as a function of σ_{x0} is shown in Fig. 12(a) as the solid lines, which scales as $\simeq 2(2/\sigma_{x0})^{1/2}$ and indicates a more severe pressure depletion in the large σ_{x0} limit, capturing the decreasing trend of simulated X-line pressure, as shown by symbols.

Meanwhile, using the force balance along the inflow symmetry line within the diffusion region (ignoring the inflow inertia in Eq. (23)), one can relate the separatrix slope to the pressure difference (between the X-line and upstream region), that is $P_{zz}|_{xline}$ (Eq. (28)) in the cold upstream limit,

$$S^2_{lope} \approx 1 - \frac{8\pi P_{zz}|_{xline}}{B^2_{xm}}. \tag{29}$$

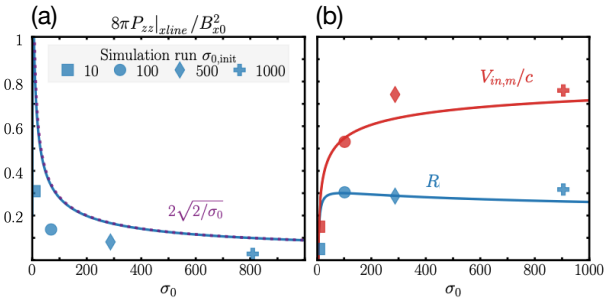

Fig. 12 First-principles theory. (a) the predicted x-line pressure as a function of σ_{x0}; (b) the predicted reconnection rate as a function of σ_{x0}. Adapted from Goodbred and Liu (2022).

Since the upstream magnetic field line adjacent to the separatrix tends to straight out (when possible, due to the magnetic tension), we can then couple this diffusion region solution to the larger upstream solution in the mesoscale, using Eq. (27) (along with Eqs. (25), (26), (24) and $B_{zm}/B_{xm} \simeq S_{lope}$) to derive the reconnection rate. The prediction of R is shown in Fig. 12(b) as the solid blue curve, which agrees well with the simulated reconnection rates (shown as symbols).

3.3 Bursty Nature of Relativistic Reconnection

Most existing literature has focused on the application of plasmoid formation in astrophysics systems and its implication for particle acceleration. As to the origin of these plasmoids in PIC simulations, does it really resemble the "high-Lindquist number plasmoid instability" derived in the uniform resistivity MHD model (Bhattacharjee et al, 2009; Loureiro et al, 2007; Shibata and Tanuma, 2001b)? The physics of the tearing instability can be different in collisionless plasmas. In addition, Hoshino (2020) shows that the collisionless tearing instability can actually be stabilized by the relativistic drift of current carriers, that was not captured in the resistive MHD model. It is plausible that, in collisionless pair plasmas, secondary plasmoids are generated because the pressure within the reconnection exhausts is also depleted in the nonlinear stage, as shown in the middle panel of Fig. 11; thus, plasmoids are violently produced from the collapse of the unbalanced current sheet. The formation of plasmoids helps balance the force, but only temporarily because they will be expelled out by outflows of the primary X-line. The evolution is settled into such a repetitive, dynamical balance. These provide an alternative explanation to the bursty nature of relativistic reconnection in the antiparallel limit, as shown in the time-stack plot in the bottom panel of Fig. 11. It is interesting to note that a similar bursty nature was also reported in two-fluid simulation (Zenitani et al, 2009a) in Fig. 7 of Section 2.5. Liu et al (2020) further demonstrated that the generation of secondary plasmoids can be suppressed in the presence of external guide fields, which is also not expected in the MHD model. As a

potential application in plasma astrophysics, the mergers of secondary plasmoids are proposed to be a plausible generation mechanism of Fast Radiation Bursts (FRB) from neutron star magnetospheres (Philippov et al, 2019).

3.4 3D Relativistic Turbulent Reconnection

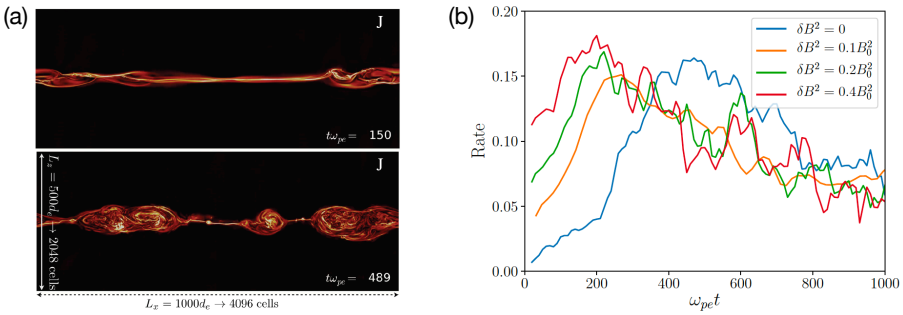

Fig. 13 Relativistic turbulent 3D reconnection in electron-positron (pair) plasmas and its reconnection rates. Panel (a) shows the current density during turbulent reconnection at two different times; Panel (b) shows the evolution of the reconnection rate in cases with different initial turbulent fluctuation levels. Note the rates are bounded by the predicted maximum plausible value even with a strong fluctuation. [Adapted from Guo et al (2021), reproduced by permission of the AAS]

The discussion thus far in this section focuses on the features in 2D kinetic simulations. It is interesting to explore the difference and similarities in a 3D system where the current sheet coexists with background turbulence. Figure 13 shows an example of relativistic turbulent reconnection in a 3D electron-positron plasma PIC simulation (Guo et al, 2021, also see Fig. 19). Fig. 13(a) shows the current density at two different times. The reconnection layer becomes highly structured because of the turbulent fluctuations initially imposed and the self-driven turbulence arising from secondary oblique tearing instability (Daughton et al, 2011) and flux-rope kink instability (Zhang et al, 2021c, 2022b). Fig. 13(b) shows the evolution of the global reconnection rates in runs with different turbulence fluctuation levels. Interestingly, no matter how strong the imposed turbulence fluctuation is, the reconnection rate is still well-bounded by the value of 0.2, as predicted by the maximum plausible rate in Section 3.2.1. A similar result was demonstrated in resistive MHD simulations (Yang et al, 2020). Unlike the "decaying turbulence setup" in Fig. 13, in Yang et al (2020), the background turbulence of different strengths is constantly driven within the system. Intriguingly, the maximum rate is still well-bounded by a similar value. Turbulent reconnection in these simulations still develops large-scale, coherent inflows and outflows. We anticipate that the force balance and the global geometrical constraint still apply on average. Analytically, one can show that the prediction in Section 3.2.1 will work, as long as the outflow speed is on the order of ion Alfvén speed (Liu et al, 2017), no

matter how thick (Lin et al, 2021; Liu et al, 2018) and complex the diffusion region is. Even though a thick turbulent diffusion region was theorized (Lazarian and Vishniac, 1999), the reconnection process in 3D PIC simulations, in fact, is still dominated by a few active diffusion regions in the kinetic scale, as also seen in Fig. 13(a). As long as the current sheet is in kinetic scale, the localization mechanism based on the fast drifting current carriers and pressure depletion, discussed in Section 3.2.2, should also work; and this will lead to fast reconnection. Nevertheless, a full resolution to this complex setting remains largely unknown, and there are several other competing ideas on turbulent reconnection (Lazarian and Vishniac, 1999; Eyink et al, 2011; Boozer, 2012; Higashimori et al, 2013); this topic is an active research area of great interest.

4 Plasma Heating and Particle Acceleration

Since magnetic reconnection in the magnetically dominated regime is likely associated with strong energy release, the heating and nonthermal particle acceleration during reconnection is of strong interests. The past two decades have witnessed unprecedented progress in our understanding of nonthermal particle acceleration in relativistic magnetic reconnection. An important discovery is that relativistic magnetic reconnection support strong particle acceleration and development of power-law energy distribution (Zenitani and Hoshino, 2001; Sironi and Spitkovsky, 2014; Guo et al, 2014, 2015; Werner et al, 2016). These discoveries are first found in the highly relativistic pair plasma and later in the mildly relativistic regime. This development also motivates the new studies in the nonrelativistic low-β regime (Li et al, 2019; Zhang et al, 2021c; Arnold et al, 2021).

4.1 Basic Acceleration Mechanisms

The basic acceleration mechanisms during magnetic reconnection can be broadly categorized into two types. The ones that accelerate particles via non-ideal electric fields and the ones via the motional electric fields $\mathbf{E} = -\mathbf{V} \times \mathbf{B}/c$. PIC simulations have uncovered several basic acceleration mechanisms such as Fermi-type acceleration, acceleration at X-line regions, and betatron acceleration, etc. In addition, analytical theories have been proposed and built to understand the acceleration processes and the resulting energy spectra.

Figure 14 shows a broad reconnection region where several acceleration mechanisms may occur. At X-points, the ideal Ohm's law is broken and strong non-ideal electric field exists $E \sim RB_0$, where R is the reconnection rate. In relativistic magnetic reconnection without a guide field, X-point acceleration is often approximated by regions where the electric field is stronger than the reconnecting magnetic field $E > B$ (Zenitani and Hoshino, 2001; Sironi and Spitkovsky, 2014). However, significant acceleration has also been found in the broader region of reconnection layer (Zenitani and Hoshino, 2007; Guo et al, 2019). Guo et al (2014, 2015) proposed that Fermi acceleration due to curvature drift motions in contacting and merging magnetic lands (similar to

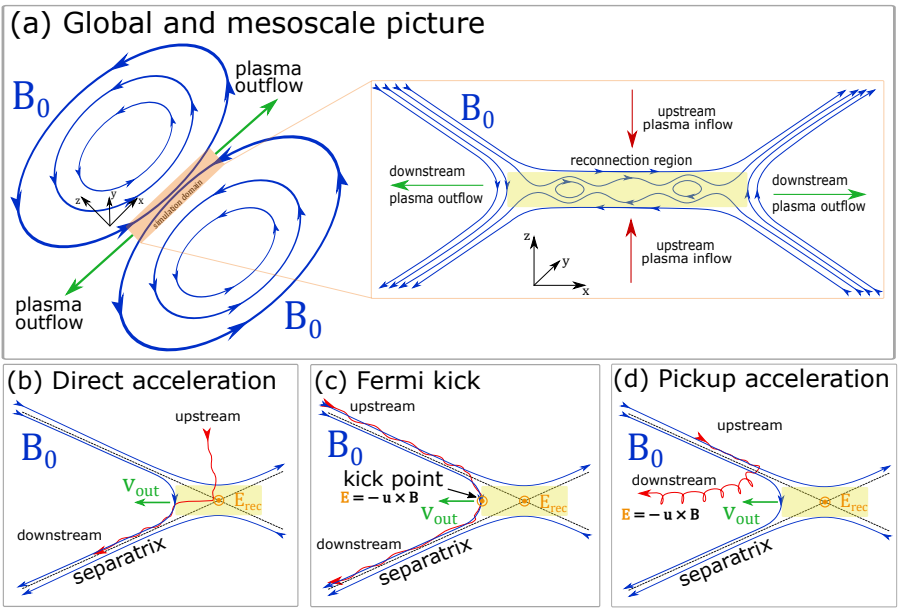

Fig. 14 Sketches of global and mesoscale reconnection configurations and several particle injection mechanisms [adapted from French et al (2023), reproduced by permission of the AAS]. (a) The surrounding astrophysical context of the reconnection region (highlighted in orange). (b) Direct acceleration from the reconnection electric field near an X-point. (c) Fermi acceleration in the exhaust region (d) Acceleration by the pickup process, where the particle becomes unmagnetized as it crossed the exhaust boundary. In panels (b-d), B_0 is the reconnecting magnetic field, $E_{\rm rec}$ is the reconnection electric field, and $v_{\rm out} \simeq v_{Ax}$ is the reconnection outflow speed, approximately equal to the in-plane Alfvén speed.

Drake et al (2006), proposed in nonrelativistic reconnection). They compared the acceleration of the parallel electric field and Fermi acceleration due to curvature drift acceleration, and found Fermi acceleration plays a dominant role. While the whole reconnection domain may have a negative contribution of betatron acceleration due to the strong energy release (decaying magnetic field $\partial B/\partial t < 0$), betatron acceleration may still be important in the converging islands (Hakobyan et al, 2021). In addition, the so-called pickup process, where particle becomes unmagnetized when entering the reconnection layer and gain energy in the outflow (Sironi and Beloborodov, 2020; French et al, 2023), can be important for low-energy acceleration.

There has been recent effort evaluating the relative importance of each mechanism (Guo et al, 2014, 2015; Kilian et al, 2020; Sironi, 2022; Guo et al, 2023; French et al, 2023). One possible way to distinguish different acceleration mechanisms is to decompose the electric field into the components perpendicular and parallel to the magnetic field ($E_\perp$ and $E_\parallel$) (Dahlin et al, 2014; Ball

et al, 2019; Kilian et al, 2020), or the motional electric field and non-ideal electric field (Guo et al, 2019)[3]. As mentioned above, the $E > B$ regions may better represent the X-point for a vanishing guide field. The analyses generally show that the acceleration associated with motional electric field (or perpendicular electric field, Fermi/betatron or pickup process) dominates for a weak guide field and weakens for stronger guide field (French et al, 2023), likely because of the compressibility of the layer (Li et al, 2018a). The contribution of the perpendicular electric field also increases with the domain size. It is important to recognize that, during magnetic reconnection, most energy conversion is through a large-scale process by the magnetic tension release, rather than at small kinetic scales. Since the nonthermal particles take a large fraction of the released energy in relativistic reconnection, they must somehow 'tap' the motional electric field. The mechanisms like Fermi acceleration would correspond to the motional electric field and therefore must be responsible to the main part of the nonthermal spectra.

Fermi acceleration can be more generalized in reconnection systems (Hoshino, 2012; Lemoine, 2019). de Gouveia dal Pino and Lazarian (2005) and Drury (2012) proposed a model considering the net compression in a reconnection layer and effect of escape. Instead of Fermi acceleration by magnetic islands, here particles are accelerated in the electric field induced by the reconnection inflow. Future studies are needed to show which Fermi acceleration is the most dominant one.

4.2 Nonthermal Acceleration uncovered by PIC simulations

Early PIC simulations show that the energy spectrum at the x-point resemble a power-law distribution (Zenitani and Hoshino, 2001), whereas the energy distribution over the broader reconnection layer is much softer (Zenitani and Hoshino, 2007). Recent large-scale PIC simulations of relativistic magnetic reconnection show a power-law energy spectrum $f(\gamma - 1) \propto \mathcal{E}^{-p}$ when integrated over the whole reconnection region with various spectral indices p as hard as $p \sim 1$ (Sironi and Spitkovsky, 2014; Guo et al, 2014, 2015; Werner et al, 2016). The nonthermal spectra have been also discussed for proton-electron plasmas, but with a reduced σ as $\sigma \sim \sigma_i \sim \sigma_e/(m_i/m_e)$ (Werner et al, 2018; Ball et al, 2018; Kilian et al, 2020; Li et al, 2023). In this regime, the energy spectra became softer ($p \gtrsim 2$). This trend naturally connects to the results from nonrelativistic reconnection, where the power-law spectra are much softer ($p \gtrsim 3 - 4$) (Li et al, 2019; Arnold et al, 2021; Zhang et al, 2021c).

As shown in Fig. 15, the nonthermal signatures found in PIC simulations can be understood in several aspects. A remarkable clear nonthermal power-law distribution is observed starting from a Lorentz factor a fraction of σ to high energy. We term this lower-energy bound as the injection energy γ_{inj}, above

[3]As discussed in Lemoine (2019), any perpendicular electric field satisfying $\mathbf{E} \cdot \mathbf{B} = 0$ and $E^2 - B^2 < 0$ may support a generalized Fermi acceleration. The speed of the collision center is not necessary the speed of the MHD flow.

which particles are accelerated into the nonthermal energies. This transition energy is also important for understanding the partition between thermal and nonthermal distribution (Hoshino, 2023; French et al, 2023). As guide field becomes stronger, the energy spectra are softer and the high-energy cutoff is suppressed (French et al, 2023). Finally, the energy spectra roll over at high energy and the cutoff energy γ_c scales with the simulation domain and time (Petropoulou and Sironi, 2018; French et al, 2023).

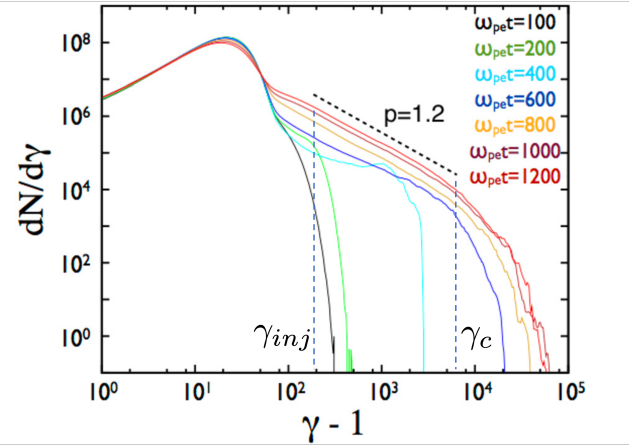

Fig. 15 The resulting energy spectrum in relativistic pair plasma reconnection from a sample PIC simulation starting from a force-free current sheet with $\sigma = 3200$ at different time steps generated from the simulation (adapted and modified from Guo et al (2020).

4.3 Physics that determine the acceleration results

The strong nonthermal features in the particle energy spectra indicate several key processes, including how particle energization transits from thermal to nonthermal energies ("injection"), how power-law energy spectra develop ("power-law formation"), and the high-energy extension of the power-law ("roll over"). Below we review the progress in understanding how they determines the energy spectra.

4.3.1 Formation of Nonthermal Power-law Energy Spectra

Can magnetic reconnection support a clear nonthermal power-law spectrum, and if so, by what mechanism and under what condition? This has been a major theoretical issue in the particle energization during magnetic reconnection (Drake et al, 2013; Guo et al, 2014).

Zenitani and Hoshino (2001) proposed a simple power-law model. Around the reconnection site, a particle is directly accelerated by the reconnection electric field $E_{\rm rec}$ in the out-of-plane direction, perpendicular to the reconnection

plane. Then its energy gain is approximated by

$$\frac{d\mathcal{E}}{dt} = eE_{\rm rec}c. \tag{30}$$

They also estimate the loss rate of particles. Since particles travel through (relativistic) Speiser motion, their typical time scale $\tau(\mathcal{E})$ in the reconnection site can be approximated by a quarter-gyration by a typical reconnected magnetic field $\bar{B}_z$. Then the particle loss rate is estimated by

$$\frac{1}{N}\frac{dN}{dt} = -\frac{4}{2\pi}\left(\frac{e\bar{B}_z}{\gamma mc}\right) = -\frac{2ce\bar{B}_z}{\pi\mathcal{E}} \tag{31}$$

A key point is that the loss rate is energy-dependent. Because of larger inertia γm, higher-energy particles are less likely to escape from the acceleration site. Combining Eqs. (30) and (31), we see that the particle number density follows the power-law distribution,

$$N \propto \mathcal{E}^{-(2\bar{B}_z)/(\pi E_{\rm rec})} \tag{32}$$

Since $\bar{B}_z/B_0 \sim \mathcal{O}(0.1)$ and $E_{\rm rec}/B_0 \sim \mathcal{O}(0.1)$, we see that the power-law index is on an order of $\mathcal{O}(1)$. Similar models have been further developed by Uzdensky (2022) and Zhang et al (2023), including magnetic flux ropes/islands as an escape region.

Recently, several new works discussed the formation of power-law distributions in a broad reconnection layer. Sironi and Spitkovsky (2014) have proposed that the power-law form is established as the particles accelerated at the X-points with $E > B$. They argue that this process is essential for the power-law formation and determines the spectra index of the energy spectra. However, since Fermi/betatron acceleration is the dominant acceleration in the board reconnection region, it is unclear how X-point acceleration can solely determine the formation of the power law. Guo et al (2014, 2015) proposed that the power-law distributions are produced by a Fermi-like process and continuous injection. In general, one can evaluate a Fokker-Planck-like equation for a reconnection layer (Guo et al, 2020; Li et al, 2021, 2023)

$$\partial_t f + \partial_{\mathcal{E}}(\alpha_{\rm acc}\mathcal{E}f) = \partial^2_{\mathcal{E}}(D_{\mathcal{E}\mathcal{E}}f) - \alpha_{\rm esc}f + \frac{f_{\rm inj}}{\tau_{\rm inj}}, \tag{33}$$

where $\mathcal{E} = (\gamma - 1)mc^2$ is the kinetic energy, $\alpha_{\rm acc}$ is the acceleration rate, $D_{\mathcal{E}\mathcal{E}} = D_0\mathcal{E}^2$ is the energy diffusion coefficient, $\alpha_{\rm esc} \equiv \tau_{\rm esc}^{-1}$ is the escape rate, $f_{\rm inj}$ is the injected particle distribution, and $\tau_{\rm inj}$ is particle injection time scale. $\alpha_{\rm acc} = (\partial_t\mathcal{E} + \partial_{\mathcal{E}}D_{\mathcal{E}\mathcal{E}})\mathcal{E}^{-1}$ describes a combination of the first-order Fermi processes and the accompanying first-order term associated with second-order Fermi mechanisms.

As reconnection proceeds, the ambient plasma continuously flows into the reconnection layer through an inflow speed V_{in} and undergo a selective injection process. For a simple case with $D_{\mathcal{E}\mathcal{E}} = 0$, the solution of (5) naturally recovers the classical solution $p = 1 + 1/(\alpha\tau_{esc})$. A power-law distribution can form from a upstream thermal distribution when $\alpha\tau$ is large (τ is the duration of acceleration) (Guo et al, 2014, 2015). In the limit that α is large, the spectral index approaches $p = 1$, consistent with existing PIC simulations. It was usually argued that an escape mechanism is necessary for forming a power-law distribution. This statement is incorrect, or at least misleading. The power-law distribution can still form even for the case with no escape term (Guo et al, 2014, 2015). The main physics for forming a power-law is due to the continuous injection and Fermi acceleration. However, it is still important to understand the escape term, as it determines the shape of the distribution. Other acceleration can in principle form a power-law, as long as the combined spectral index p does not depend on energy.

$$p = 1 + \frac{1}{\alpha\tau_{esc}} + \frac{\partial \ln \alpha}{\partial \ln \epsilon} = \text{const.} \tag{34}$$

Hakobyan et al (2021) has developed an analytical model based on betatron acceleration to explain the high-energy nonthermal part of the spectra. Li et al (2023) measured the acceleration and escape rates in PIC simulations and the numerical solution of Eq. 33 achieved a nice agreement with the PIC simulation results.

4.3.2 Energy Partition of Thermal and Nonthermal Particles in Reconnection

Magnetic reconnection is known to be the most important mechanism not only for plasma thermalization up to the equivalent temperature of the Alfvén velocity, but also for accelerating nonthermal particles whose energies exceed their thermal energies (e.g., Birn and Priest, 2007; Zweibel and Yamada, 2009; Hoshino and Lyubarsky, 2012; Uzdensky, 2016; Blandford et al, 2017). It was known that non-negligible fraction of nonthermal particle is generated during reconnection through satellite observations of the Earth's magnetosphere and the solar atmosphere (e.g., Øieroset et al, 2002; Lin et al, 2003) and PIC simulation studies for non-relativistic plasmas (e.g., Pritchett, 2001; Hoshino et al, 2001; Drake et al, 2006; Oka et al, 2010). Furthermore, as magnetic reconnection is an ubiquitous process in the plasma universe, reconnection is believed to occur in many high-energy astrophysical phenomena such as in pulsar magnetosphere, accretion disks, and magnetar (e.g., Remillard and McClintock, 2006; Done et al, 2007; Madejski and Sikora, 2016; Kirk, 2004; Lyutikov and Uzdensky, 2003). PIC simulation studies also revealed that relativistic reconnection whose Alfvén velocity is close to the speed of light can effectively generate nonthermal particles with a harder power-law energy spectrum than that generated in non-relativistic plasmas (e.g. Zenitani and Hoshino, 2001, 2005a,b; Jaroschek et al, 2004; Jaroschek and Hoshino, 2009; Cerutti et al, 2012a,b,

2013; Liu et al, 2011; Sironi and Spitkovsky, 2011, 2014; Guo et al, 2014). Since then, regardless of whether the plasma is nonrelativistic or relativistic, magnetic reconnection has gained attention as a mechanism of nonthermal particle acceleration in various space and astrophysical sources. However, the energy partitioning of thermal and nonthermal plasmas during magnetic reconnection is not understood. The energy partition plays an important role on the dynamical evolution of magnetic reconnection.

Recently, the energy partitioning has been quantitatively investigated by using PIC simulations for a pair plasma (Hoshino, 2022, 2023). The downstream heated plasma by reconnection has been found to be well modeled by a composed distribution function consisting of a Maxwell distribution function $N_M(\gamma)$ and a kappa distribution function $N_\kappa(\gamma)$, where $N_M(\gamma) = n_M\gamma\sqrt{\gamma^2-1}\exp(-(\gamma-1)/(T_M/mc^2))$, and $N_\kappa(\gamma) = n_\kappa\gamma\sqrt{\gamma^2-1}\left(1+(\gamma-1)/(\kappa T_\kappa/mc^2)\right)^{-(1+\kappa)} f_{cut}(\gamma)$. (It is interesting to note that the kappa distribution function can be widely observed in space plasma environments (Vasyliunas, 1968; Livadiotis and McComas, 2013), and the formation of the kappa distribution function may be related to the idea of non-extensive statistics (Tsallis, 1988).) Based on the model fitting, Figure 16 shows (a) the average thermal temperature of the Maxwellian and κ functions, which is described as $T_{th} = (n_M T_M + n_\kappa T_\kappa)/(n_M + n_\kappa)$, (b) κ index, and (c) the fraction of the nonthermal energy density $\mathcal{E}_{\rm ene}$ as a function of the plasma temperature (T_0/mc^2) and guide field (B_G/B_0). The nonthermal fraction $\mathcal{E}_{\rm ene}$ is defined as $\mathcal{E}_{\rm ene} = \int_1^\infty(\gamma-1)(N_\kappa(\gamma) - N_\kappa^{\rm M}(\gamma))d\gamma / \int_1^\infty(\gamma-1)N_{{\rm M}+\kappa}(\gamma)d\gamma$, where $N_\kappa^{\rm M}(\gamma)$ represents the portion of the Maxwellian distribution function in the κ distribution function. For anti-parallel magnetic field topology without a guide magnetic field, it was found that while the nonthermal energy density in relativistic reconnection can occupy more than 90% of the total kinetic plasma energy density, most dissipated magnetic field energy can be converted into thermal plasma heating in nonrelativistic reconnection. For magnetic reconnection with a guide magnetic field, it is found that the efficiency of nonthermal particle acceleration was enhanced for nonrelativistic reconnection with a weak guide field. However, for both nonrelativistic and relativistic reconnections, the efficiency of stronger guide-field reconnection was suppressed. In the relativistic regime, a recent study by French et al (2023) determines an injection energy beyond which the particle energy distribution are well described by a power-law spectrum. They define the acceleration efficiency by the "number" and "energy", where the contribution of downstream nonthermal particles over the total downstream population are calculated. Consistently they find that stronger guide field suppresses the efficiency and the efficiency may saturate to a final asymptotic value for a sufficiently large domain (see Fig. 17).

4.3.3 Injection problem

There has been several studies on the injection problem with energization up until the injection energy γ_{inj}. While Ball et al (2019) focused on the work done by the parallel electric field ($W_\parallel$), Kilian et al (2020) studied the roles of

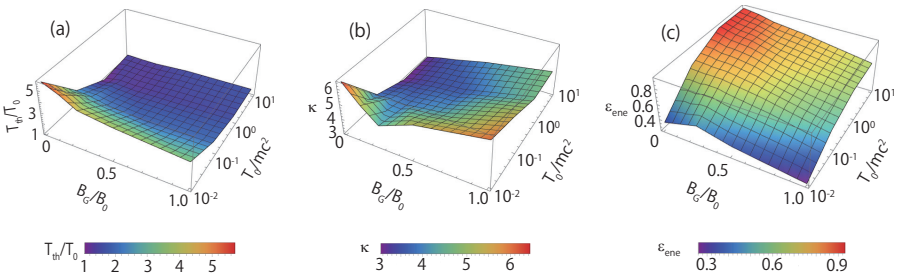

Fig. 16 Model fitting results as functions of the initial plasma temperatures $T/mc^2 = 10^{-2} \sim 10^1$ and the guide magnetic fields of $B_G/B_0 = 0 \sim 1$. Three panels show (a) the average temperatures normalized by the initial background temperature T_0, (b) κ index, and (c) efficiency of nonthermal particles against thermal plasmas as a function of the initial plasma temperature T/mc^2 and guide magnetic field B_G/B_0. Adapted from Hoshino (2023), reproduced by permission of the AAS].

both parallel and perpendicular electric field. They showed that both parallel and perpendicular electric fields play a role and perpendicular electric field becomes more important for particle injection, especially when the simulation domain becomes large. While acknowledging the importance of $W_\perp$ during the development of the power-law distribution, Sironi (2022) further suggest $E > B$ regions are important for injecting particles by accelerating particles and they claimed all injected particles need to cross the x-points. This apparent correlation is further studied by Guo et al (2023), and importantly, shown to have no significant contributions to the injection process. Guo et al (2023) showed that $E > B$ regions contribute very little to injection ($\sim 10\%\gamma_{inj}$) as they only host particles for a short time, insufficient for boosting the particles to injection. French et al (2023) studied three different injection mechanisms (parallel electric field, Fermi reflection, and pickup process) and attempted to quantify their relative importance. Figure 18 shows that the Fermi and pickup processes, related to the electric field perpendicular to the magnetic field, govern the injection for weak guide fields and larger domains. Meanwhile, parallel electric fields are important for injection in the strong guide-field regime.

4.3.4 High-energy roll-over

Early results with weak guide field show that the spectral index can be as hard as $p \sim 1$ for high σ, meaning the energy contained in such a spectrum is dominated by high-energy particles, thus energy starving and is limited by the amount of dissipated magnetic energy $\gamma_c \sim [2\delta\sigma(2-p)]^{1/(2-p)}$, where δ is the fraction of the dissipated magnetic energy channeled into each species. For $p \sim 1$ this gives a high-energy roll-over at a few times σ (Werner et al, 2016). It was suggested that as reconnection proceeds, the acceleration may evolve into a softer spectra ($p \sim 2$) and the high-energy acceleration can proceed for a long time (Petropoulou and Sironi, 2018; French et al, 2023), although the σ dependence still exists. Meanwhile, a stronger guide field or escape effects would make a difference. A significant guide field leads to a softer

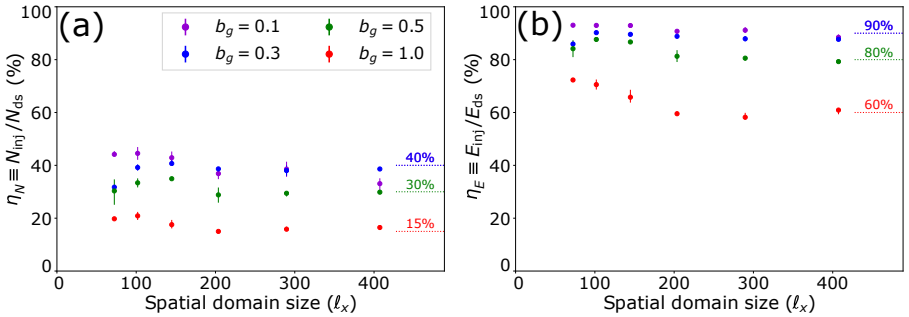

Fig. 17 Acceleration efficiencies from PIC simulations adapted from French et al (2023), reproduced by permission of the AAS. (a) The number efficiency (the ratio between injected particle number to the downstream particle number) $\eta_N \equiv N_{\rm inj}/N_{\rm ds}$. (b) The energy efficiency $\eta_E \equiv E_{\rm inj}/E_{\rm ds}$ for the ratio between the sum of injected particle energy to the energy of the whole downstream population).

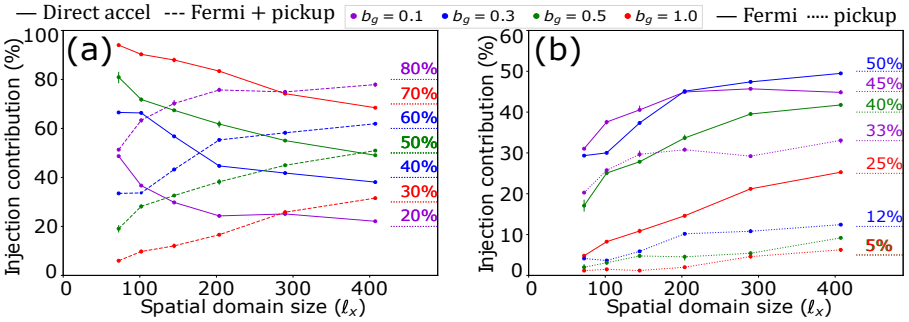

Fig. 18 Cumulative percentage of injected electrons that are injected by each particle acceleration mechanism ((French et al, 2023), reproduced by permission of the AAS]). (a): Decomposition between particles injected by $W_{\parallel}$ (solid) and $W_{\perp}$ (dashed). (b): Decomposition between Fermi-injected particles (solid) and pickup-injected particles (dotted).

spectrum and lower the maximum energy (French et al, 2023; Li et al, 2023). As reconnection proceeds, escape process needs to be considered to correctly understand high-energy roll-over.

4.4 The Roles of 3D reconnection and turbulence

Earlier discussion on 3D relativistic reconnection primarily focused on the drift kink instability (Zenitani and Hoshino, 2007; Liu et al, 2011). However, the flux rope kink instability can also grow and drive turbulence (Zhang et al, 2021c; Guo et al, 2021). Both of these can be suppressed by a strong guide field (Zenitani and Hoshino, 2008). In the strong guide field regime, the oblique tearing instability is likely dominant (Guo et al, 2021). As instabilities evolve, it is well established that 3D reconnection can spontaneously generate magnetic turbulence (See Figure 19). Recent 3D studies have shown that 3D effects can be important for efficient acceleration in reconnection (Dahlin et al, 2017; Li

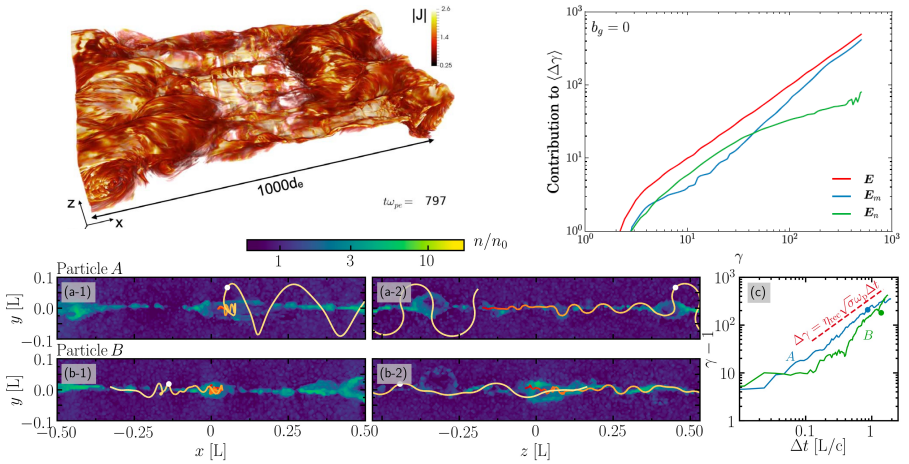

Fig. 19 Several recent studies on 3D relaltivistic magnetic reconnection and associated particle acceleration. Upper panels: The reconnection layer becomes significantly turbulent as the flux rope kink instability grows. The acceleration to high energy is dominated by the motional electric field ($\mathbf{E}_m$) and the non-ideal electric field ($\mathbf{E}_n$) plays a subdominant role (adapted from (Guo et al, 2021). Lower panels: 3D relativistic reconnection supports additional acceleration pattern, as particles can meander across the reconnection and gain energy in the upstream electric field (Zhang et al, 2021b). Figures reproduced by permission of the AAS.

et al, 2019; Zhang et al, 2021c, 2022a). In 2D magnetic field configuration particles are trapped in magnetic islands due to restricted particle motion across magnetic field lines (Jokipii et al, 1993; Jones et al, 1998; Giacalone et al, 1994; Johnson et al, 2022), and high-energy particle acceleration can be prohibited. Chaotic field lines and turbulence due to the 3D evolution of the oblique tearing instability (e.g., Daughton et al, 2011; Liu et al, 2013) and flux rope kink instability (e.g., Guo et al, 2021; Zhang et al, 2021c) make particles leave the flux rope and can lead to efficient transport of particles in the reconnection region, which is found to be important for further acceleration in the reconnection region (Dahlin et al, 2017; Li et al, 2019). The most recent work by Zhang et al (2022a) shows that particles can escape from flux ropes and get acceleration in the reconnection inflow regions via Speiser-like orbits (Figure 19).

4.5 The problem of scale separation and macroscopic approach

PIC simulations have developed to a point that it is very useful to study the elementary processes of relativistic magnetic reconnection and particle acceleration (see Shay et al. this collection), and they have been used to explore the global physics. However, one should remember that the scale separation in astrophysical problems is far beyond the reach of PIC simulations. For example, the ratio between the system size and the plasma skin depth can be

$\sim 10^{13} - 10^{17}$ for pulsar wind nebulae and extragalactic jets. The conclusions made by PIC simulations need to be extrapolated to large scale, and it is unknown if all the conclusions can still hold in large scale. The solution to this serious issue is to develop a large-scale model that contains basic acceleration physics learned from PIC simulations.

At large scales where the domain of the reconnection layer becomes much larger than the gyromotion scale, one often can use the guiding center approximation, which includes Fermi/betatron acceleration identified as primary acceleration mechanisms (Guo et al, 2014; Dahlin et al, 2014; Li et al, 2017). An alternative solution is to use energetic particle transport theory. Li et al (2018a) have shown that the acceleration in the reconnection layer can be described as compression and shear, which are main acceleration physics included in the energetic particle transport theory (Parker, 1957, 1965; Zank, 2014; le Roux et al, 2015). This approach has been used to study large-scale reconnection acceleration (Li et al, 2018b, 2022). In addition, Fermi acceleration can be studied by following the momentum changes of particles through a sequence of local frames where the local electric field vanishes (Lemoine, 2019). Monte Carlo simulations (e.g., Seo et al, 2022) including this description may alleviate the complicity of the particle transport equations, when the plasma flow becomes relativistic (Webb, 1989).

PIC simulations show that nonthermal particles can take a significant energy of the system, and therefore it may be important to include the feedback of energetic particles. Drake et al (2019) presented a set of equations where the guiding-center particles feedback in the MHD equations so the total energy of the system for the fluid and 'hot' particles is conserved. The feedback is through the pressure tensor of the energetic particles in the fluid equations. Arnold et al (2021) successfully showed magnetic islands in reconnection layer accelerate particles via Fermi acceleration and lead to the development of power-law energy spectra. This description has not included the effect of particle scattering in turbulence, which is expected to be important in 3D turbulent reconnection. An alternative (equivalent) way to include the feedback is through the electric current carried by energetic particles (Bai et al, 2015; Sun and Bai, 2023).

5 Final Remarks

This review summarizes recent progress in relativistic magnetic reconnection, focusing on its fluid description and simulations, collisionless reconnection physics, and particle energization. We remark several directions that will become frontier problems and need further attentions.

One of the most important topics is 3D magnetic reconnection. Although many scientists have studied reconnection in 2D and 3D, the 3D evolution is still an open issue. At this point, it is unclear whether magnetic reconnection always proceeds through a thin layer on the kinetic or resistive scale.

It is widely believed that the coupling between magnetic reconnection/tearing instability and current-driven instabilities such as the drift-kink instability play an important role in the formation of turbulent current sheets. When 3D turbulence broaden the kinetic layer, its subsequent evolution can be sensitive to the current-sheet and ambient plasma parameters. The 3D system evolution inevitably influences the way particles are accelerated, and therefore we need to clarify whether particle acceleration in 3D is fundamentally different from that in 2D. These aspects have not been settled, and future progress is still very much needed to gain further insights.

As will be discussed in another article (Nakamura et al., 2023, this issue), it is important to understand the onset mechanism of magnetic reconnection. Kinetic simulations typically start from a thin and long Harris sheet in relativistic reconnection problems, but the current sheet is highly unstable to kinetic instabilities which grow in a few gyroperiods. Then, it is not clear whether the Harris sheet is the best initial condition. In order to justify many earlier works, or in order to discover the best initial condition, we demand more research on the formation and stability of the "initial" current sheet.

In the future, in order to study the magnetosphere or even larger systems, we need to simultaneously resolve kinetic scales of magnetic reconnection near the central object and the large-scale evolution of the entire system. Numerical simulation across such many scales will be challenging, in particular in astrophysical settings. To deal with the cross-scale problem, several attempts have been made to interconnect small-scale kinetic simulations and large-scale MHD simulations (Sugiyama and Kusano, 2007; Usami et al, 2013; Daldorff et al, 2014) for nonrelativistic problems, however, the number of these MHD-PIC models is very limited. Unfortunately, no similar attempts have been reported in relativistic astrophysics, partly because it is difficult to translate kinetic quantities into fluid quantities as discussed in Section 3. A lot more work is necessary to develop relativistic MHD-PIC models. As we have discussed in Section 4.5, it is important to consider nonthermal particle acceleration in MHD models, studying and predicting energetic particles and their signatures in large-scale systems.

Beyond the description discussed in this review article, incorporating the radiation (Jaroschek and Hoshino, 2009; Cerutti et al, 2013; Zhang et al, 2018; Werner et al, 2019; Sironi and Beloborodov, 2020; Schoeffler et al, 2023) and other QED processes (Schoeffler et al, 2019), such as pair production and annihilation, during reconnection is also important for one to delve into the rich physics in such extreme astrophysical plasmas. On the other hand, this endeavor could also help extract observable signatures for distant observers, constraining our understanding of relativistic magnetic reconnection.

With recent breakthroughs, relativistic magnetic reconnection has become an important topic in reconnection studies and a key process for understanding astrophysical energy release, particle acceleration, and high-energy radiation. Although difficult, it is highly anticipated that transformative progress will be achieved in the near future in key areas (Section 1.2) of relativistic magnetic

reconnection, reaching a more complete physics understanding, achieving a more advanced modeling capability, and better connecting with astrophysical observations.

Acknowledgments. F. G. acknowledges the support from Los Alamos National Laboratory through the LDRD program, DOE Office of Science, and NASA programs through the Astrophysical Theory Program. The work by Y. L. is funded by the National Science Foundation grant PHY-1902867 through the NSF/DOE Partnership in Basic Plasma Science and Engineering and NASA 80NSSC21K2048. The work by S. Z. was funded by Japan Society for the Promotion of Science (JSPS) KAKENHI, Grant No. 21K03627. The work by M. H. was supported by JSPS KAKENHI, Grant Nos. 19H01949 and 20K20908.

Conflict of interest. The authors have no conflict of interest to declare that is relevant to the content of this article.

References

Abdo AA, Ackermann M, Ajello M, et al (2011) Science, 331(6018):739. https://doi.org/10.1126/science.1199705, [astro-ph.HE]

Abeysekara AU, Albert A, Alfaro R, et al (2017) Science, 358(6365):911–914. https://doi.org/10.1126/science.aan4880, [astro-ph.HE]

Ackermann M, Anantua R, Asano K, et al (2016) Astrophysical Journal Letters, 824(2):L20. https://doi.org/10.3847/2041-8205/824/2/L20, [astro-ph.HE]

Alves EP, Zrake J, Fiuza F (2018) Physical Review Letters, 121(24):245101. https://doi.org/10.1103/PhysRevLett.121.245101

Amano T (2016) Astrophysical Journal, 831(1):100. https://doi.org/10.3847/0004-637X/831/1/100

Arnold H, Drake JF, Swisdak M, et al (2021) Physical Review Letters, 126(13):135101. https://doi.org/10.1103/PhysRevLett.126.135101, [physics.plasm-ph]

Arons J (2012) Space Science Reviews, 173(1-4):341–367. https://doi.org/10.1007/s11214-012-9885-1

Bai XN, Caprioli D, Sironi L, et al (2015) Astrophysical Journal, 809(1):55. https://doi.org/10.1088/0004-637X/809/1/55

Ball D, Sironi L, Özel F (2018) Astrophysical Journal, 862(1):80. https://doi.org/10.3847/1538-4357/aac820

Ball D, Sironi L, Özel F (2019) Astrophysical Journal, 884(1):57. https://doi.org/10.3847/1538-4357/ab3f2e, [astro-ph.HE]

Balsara DS, Amano T, Garain S, et al (2016) Journal of Computational Physics, 318:169–200. https://doi.org/10.1016/j.jcp.2016.05.006, [physics.comp-ph]

Barkov M, Komissarov SS, Korolev V, et al (2014) Monthly Notices of the Royal Astronomical Society, 438(1):704–716. https://doi.org/10.1093/mnras/stt2247

Bhattacharjee A, Huang YM, Yang H, et al (2009) Physics of Plasmas, 16(11):112102. https://doi.org/10.1063/1.3264103, [physics.plasm-ph]

Birn J, Priest ER (2007) Reconnection of magnetic fields : magnetohydrodynamics and collisionless theory and observations. Cambridge University Press

Biskamp D (1986) Physics of Fluids, 29(5):1520–1531. https://doi.org/10.1063/1.865670

Blackman EG, Field GB (1994) Physical Review Letters, 72(4):494–497. https://doi.org/10.1103/PhysRevLett.72.494

Blandford R, Yuan Y, Hoshino M, et al (2017) Space Science Reviews, 207(1-4):291–317. https://doi.org/10.1007/s11214-017-0376-2

Bodo G, Tavecchio F, Sironi L (2021) Monthly Notices of the Royal Astronomical Society, 501(2):2836–2847. https://doi.org/10.1093/mnras/staa3620

Bohdan A, Pohl M, Niemiec J, et al (2020) Astrophysical Journal, 904(1):12. https://doi.org/10.3847/1538-4357/abbc19, [astro-ph.HE]

Boozer AH (2012) Physics of Plasmas, 19(11):112901. https://doi.org/10.1063/1.4765352

Bucciantini N, Del Zanna L (2013) Monthly Notices of the Royal Astronomical Society, 428(1):71–85. https://doi.org/10.1093/mnras/sts005, [astro-ph.HE]

Burgess D, Hellinger P, Gingell I, et al (2016) Journal of Plasma Physics, 82(4):905820401. https://doi.org/10.1017/S0022377816000660, [physics.space-ph]

Cerutti B, Uzdensky DA, Begelman MC (2012a) Astrophysical Journal, 746(2):148. https://doi.org/10.1088/0004-637X/746/2/148

Cerutti B, Werner GR, Uzdensky DA, et al (2012b) Astrophysical Journal Letters, 754(2):L33. https://doi.org/10.1088/2041-8205/754/2/L33

Cerutti B, Werner GR, Uzdensky DA, et al (2013) Astrophysical Journal, 770(2):147. https://doi.org/10.1088/0004-637X/770/2/147

Comisso L, Lingam M, Huang YM, et al (2017) Astrophysical Journal, 850(2):142. https://doi.org/10.3847/1538-4357/aa9789, [astro-ph.HE]

Coroniti FV (1990) Astrophysical Journal, 349:538. https://doi.org/10.1086/168340

Dahlin JT, Drake JF, Swisdak M (2014) Physics of Plasmas, 21(9):092304. https://doi.org/10.1063/1.4894484, [physics.plasm-ph]

Dahlin JT, Drake JF, Swisdak M (2017) Physics of Plasmas, 24(9):092110. https://doi.org/10.1063/1.4986211, [physics.plasm-ph]

Daldorff LKS, Tóth G, Gombosi TI, et al (2014) Journal of Computational Physics, 268:236–254. https://doi.org/10.1016/j.jcp.2014.03.009

Daughton W, Karimabadi H (2007) Physics of Plasmas, 14(7):072303. https://doi.org/10.1063/1.2749494

Daughton W, Roytershteyn V, Albright BJ, et al (2009) Physical Review Letters, 103(6):065004. https://doi.org/10.1103/PhysRevLett.103.065004

Daughton W, Roytershteyn V, Karimabadi H, et al (2011) Nature Physics, 7(7):539–542. https://doi.org/10.1038/nphys1965

de Gouveia dal Pino EM, Lazarian A (2005) Astronomy and Astrophysics, 441(3):845–853. https://doi.org/10.1051/0004-6361:20042590

Dedner A, Kemm F, Kröner D, et al (2002) Journal of Computational Physics, 175(2):645–673. https://doi.org/10.1006/jcph.2001.6961

Dionysopoulou K, Alic D, Palenzuela C, et al (2013) Physical Review D, 88(4):044020. https://doi.org/10.1103/PhysRevD.88.044020, [gr-qc]

Done C, Gierliński M, Kubota A (2007) Astronomy and Astrophysics Reviews, 15(1):1–66. https://doi.org/10.1007/s00159-007-0006-1, [astro-ph]

Drake JF, Swisdak M, Che H, et al (2006) Nature, 443(7111):553–556. https://doi.org/10.1038/nature05116

Drake JF, Swisdak M, Fermo R (2013) Astrophysical Journal Letters, 763(1):L5. https://doi.org/10.1088/2041-8205/763/1/L5, [astro-ph.SR]

Drake JF, Arnold H, Swisdak M, et al (2019) Physics of Plasmas, 26(1):012901. https://doi.org/10.1063/1.5058140, [astro-ph.SR]

Drury LO (2012) Monthly Notices of the Royal Astronomical Society, 422(3):2474–2476. https://doi.org/10.1111/j.1365-2966.2012.20804.x

Dumbser M, Zanotti O (2009) Journal of Computational Physics, 228(18):6991–7006. https://doi.org/10.1016/j.jcp.2009.06.009, [gr-qc]

Eckart C (1940) Physical Review, 58(10):919–924. https://doi.org/10.1103/PhysRev.58.919

Eyink GL, Lazarian A, Vishniac ET (2011) Astrophysical Journal, 743(1):51. https://doi.org/10.1088/0004-637X/743/1/51, [astro-ph.GA]

French O, Guo F, Zhang Q, et al (2023) Astrophysical Journal, 948(1):19. https://doi.org/10.3847/1538-4357/acb7dd

Giacalone J, Jokipii JR, Kota J (1994) Journal of Geophysical Research, 99(A10):19,351–19,358. https://doi.org/10.1029/94JA01213

Giannios D, Uzdensky DA, Begelman MC (2009) Monthly Notices of the Royal Astronomical Society, 395(1):L29–L33. https://doi.org/10.1111/j.1745-3933.2009.00635.x

Goodbred M, Liu YH (2022) Physical Review Letters, 129(26):265101. https://doi.org/10.1103/PhysRevLett.129.265101

Guo F, Li H, Daughton W, et al (2014) Physical Review Letters, 113(15):155005. https://doi.org/10.1103/PhysRevLett.113.155005

Guo F, Liu YH, Daughton W, et al (2015) Astrophysical Journal, 806(2):167. https://doi.org/10.1088/0004-637X/806/2/167

Guo F, Li H, Daughton W, et al (2016a) Physics of Plasmas, 23(5):055708. https://doi.org/10.1063/1.4948284

Guo F, Li X, Li H, et al (2016b) Astrophysical Journal Letters, 818(1):L9. https://doi.org/10.3847/2041-8205/818/1/L9

Guo F, Li X, Daughton W, et al (2019) Astrophysical Journal Letters, 879(2):L23. https://doi.org/10.3847/2041-8213/ab2a15

Guo F, Liu YH, Li X, et al (2020) Physics of Plasmas, 27(8):080501. https://doi.org/10.1063/5.0012094

Guo F, Li X, Daughton W, et al (2021) Astrophysical Journal, 919(2):111. https://doi.org/10.3847/1538-4357/ac0918

Guo F, Li X, French O, et al (2023) Physical Review Letters, 130(18):189501. https://doi.org/10.1103/PhysRevLett.130.189501

Hakobyan H, Petropoulou M, Spitkovsky A, et al (2021) Astrophysical Journal, 912(1):48. https://doi.org/10.3847/1538-4357/abedac

Hesse M, Zenitani S (2007) Physics of Plasmas, 14(11):112102. https://doi.org/10.1063/1.2801482

Higashimori K, Yokoi N, Hoshino M (2013) Physical Review Letters, 110(25):255001. https://doi.org/10.1103/PhysRevLett.110.255001, [astro-ph.EP]

Hoshino M (2012) Physical Review Letters, 108(13):135003. https://doi.org/10.1103/PhysRevLett.108.135003

Hoshino M (2015) Physical Review Letters, 114(6):061101. https://doi.org/10.1103/PhysRevLett.114.061101, [astro-ph.HE]

Hoshino M (2020) Astrophysical Journal, 900(1):66. https://doi.org/10.3847/1538-4357/aba59d

Hoshino M (2022) Physics of Plasmas, 29(4):042902. https://doi.org/10.1063/5.0086316

Hoshino M (2023) Astrophysical Journal, 946(2):77. https://doi.org/10.3847/1538-4357/acbfb5

Hoshino M, Lyubarsky Y (2012) Space Science Reviews, 173(1-4):521–533. https://doi.org/10.1007/s11214-012-9931-z

Hoshino M, Mukai T, Terasawa T, et al (2001) Journal of Geophysical Research, 106(A11):25,979–25,998. https://doi.org/10.1029/2001JA900052

Huang YM, Comisso L, Bhattacharjee A (2017) Astrophysical Journal, 849(2):75. https://doi.org/10.3847/1538-4357/aa906d, [physics.plasm-ph]

Inda-Koide M, Koide S, Morino R (2019) Astrophysical Journal, 883(1):69. https://doi.org/10.3847/1538-4357/ab345f, [astro-ph.HE]

Jaroschek CH, Hoshino M (2009) Physical Review Letters, 103(7):075002. https://doi.org/10.1103/PhysRevLett.103.075002

Jaroschek CH, Treumann RA, Lesch H, et al (2004) Physics of Plasmas, 11(3):1151–1163. https://doi.org/10.1063/1.1644814

Ji H, Daughton W (2011) Physics of Plasmas, 18(11):111,207–111,207. https://doi.org/10.1063/1.3647505, [astro-ph.IM]

Ji H, Daughton W, Jara-Almonte J, et al (2022) Nature Reviews Physics,

4(4):263–282. https://doi.org/10.1038/s42254-021-00419-x, [physics.plasm-ph]

Johnson G, Kilian P, Guo F, et al (2022) Astrophysical Journal, 933(1):73. https://doi.org/10.3847/1538-4357/ac7143, [astro-ph.SR]

Jokipii JR, Kota J, Giacalone J (1993) Geophysical Research Letters, 20(17):1759–1761. https://doi.org/10.1029/93GL01973

Jones FC, Jokipii JR, Baring MG (1998) Astrophysical Journal, 509(1):238–243. https://doi.org/10.1086/306480, [astro-ph]

Kato TN, Takabe H (2008) Astrophysical Journal Letters, 681(2):L93. https://doi.org/10.1086/590387, [astro-ph]

Kilian P, Li X, Guo F, et al (2020) Astrophysical Journal, 899(2):151. https://doi.org/10.3847/1538-4357/aba1e9

Kirk JG (2004) Physical Review Letters, 92(18):181101. https://doi.org/10.1103/PhysRevLett.92.181101, [astro-ph]

Kirk JG, Skjæraasen O (2003) Astrophysical Journal, 591(1):366–379. https://doi.org/10.1086/375215, [astro-ph]

Komissarov SS (2007) Monthly Notices of the Royal Astronomical Society, 382(3):995–1004. https://doi.org/10.1111/j.1365-2966.2007.12448.x, [astro-ph]

Lazarian A, Vishniac ET (1999) Astrophysical Journal, 517(2):700–718. https://doi.org/10.1086/307233, [astro-ph]

le Roux JA, Zank GP, Webb GM, et al (2015) Astrophysical Journal, 801(2):112. https://doi.org/10.1088/0004-637X/801/2/112

Lemoine M (2019) Physical Review D, 99(8):083006. https://doi.org/10.1103/PhysRevD.99.083006

Li X, Guo F, Li H, et al (2017) Astrophysical Journal, 843(1):21. https://doi.org/10.3847/1538-4357/aa745e

Li X, Guo F, Li H, et al (2018a) Astrophysical Journal, 855(2):80. https://doi.org/10.3847/1538-4357/aaacd5, [physics.plasm-ph]

Li X, Guo F, Li H, et al (2018b) Astrophysical Journal, 866(1):4. https://doi.org/10.3847/1538-4357/aae07b, [astro-ph.SR]

Li X, Guo F, Li H, et al (2019) Astrophysical Journal, 884(2):118. https://doi.org/10.3847/1538-4357/ab4268, [astro-ph.SR]

Li X, Guo F, Liu YH (2021) Physics of Plasmas, 28(5):052905. https://doi.org/10.1063/5.0047644, [physics.plasm-ph]

Li X, Guo F, Chen B, et al (2022) Astrophysical Journal, 932(2):92. https://doi.org/10.3847/1538-4357/ac6efe, [astro-ph.SR]

Li X, Guo F, Liu YH, et al (2023) Astrophysical Journal Letters, 954(2):L37. https://doi.org/10.3847/2041-8213/acf135, [astro-ph.HE]

Lin RP, Krucker S, Hurford GJ, et al (2003) Astrophysical Journal Letters, 595(2):L69–L76. https://doi.org/10.1086/378932

Lin SC, Liu YH, Li X (2021) Physics of Plasmas, 28(7):072109. https://doi.org/10.1063/5.0052317, [physics.plasm-ph]

Lin X, Li YP, Yuan F (2023) Monthly Notices of the Royal Astronomical Society, 520(1):1271–1284. https://doi.org/10.1093/mnras/stad176, [astro-ph.HE]

Liu W, Li H, Yin L, et al (2011) Physics of Plasmas, 18(5):052,105–052,105. https://doi.org/10.1063/1.3589304

Liu YH, Daughton W, Karimabadi H, et al (2013) Physical Review Letters, 110(26):265004. https://doi.org/10.1103/PhysRevLett.110.265004

Liu YH, Guo F, Daughton W, et al (2015) Physical Review Letters, 114(9):095002. https://doi.org/10.1103/PhysRevLett.114.095002

Liu YH, Hesse M, Guo F, et al (2017) Physical Review Letters, 118(8):085101. https://doi.org/10.1103/PhysRevLett.118.085101, [physics.plasm-ph]

Liu YH, Hesse M, Guo F, et al (2018) Physics of Plasmas, 25(8):080701. https://doi.org/10.1063/1.5042539, [physics.plasm-ph]

Liu YH, Lin SC, Hesse M, et al (2020) Astrophysical Journal Letters, 892(1):L13. https://doi.org/10.3847/2041-8213/ab7d3f

Liu YH, Cassak P, Li X, et al (2022) Communications Physics, 5(1):97. https://doi.org/10.1038/s42005-022-00854-x, [physics.plasm-ph]

Livadiotis G, McComas DJ (2013) Space Science Reviews, 175(1-4):183–214. https://doi.org/10.1007/s11214-013-9982-9

Loureiro NF, Schekochihin AA, Cowley SC (2007) Physics of Plasmas, 14(10):100,703–100,703. https://doi.org/10.1063/1.2783986, [astro-ph]

Lu Y, Guo F, Kilian P, et al (2021) Astrophysical Journal, 908(2):147. https://doi.org/10.3847/1538-4357/abd406

Lyubarsky Y, Kirk JG (2001) Astrophysical Journal, 547(1):437–448. https://doi.org/10.1086/318354, [astro-ph]

Lyubarsky YE (2005) Monthly Notices of the Royal Astronomical Society, 358(1):113–119. https://doi.org/10.1111/j.1365-2966.2005.08767.x, [astro-ph]

Lyutikov M, Uzdensky D (2003) Astrophysical Journal, 589(2):893–901. https://doi.org/10.1086/374808, [astro-ph]

Madejski GG, Sikora M (2016) Annual Review of Astronomy and Astrophysics, 54:725–760. https://doi.org/10.1146/annurev-astro-081913-040044

Matsumoto Y, Amano T, Kato TN, et al (2015) Science, 347(6225):974–978. https://doi.org/10.1126/science.1260168

McKinney JC, Uzdensky DA (2012) Monthly Notices of the Royal Astronomical Society, 419(1):573–607. https://doi.org/10.1111/j.1365-2966.2011.19721.x

Mehlhaff JM, Werner GR, Uzdensky DA, et al (2020) Monthly Notices of the Royal Astronomical Society, 498(1):799–820. https://doi.org/10.1093/mnras/staa2346

Mignone A, Mattia G, Bodo G, et al (2019) Monthly Notices of the Royal Astronomical Society, 486(3):4252–4274. https://doi.org/10.1093/mnras/stz1015, [physics.comp-ph]

Mizuno Y (2013) Astrophysical Journal Supplementary, 205(1):7. https://doi.org/10.1088/0067-0049/205/1/7

Munz CD, Omnes P, Schneider R, et al (2000) Journal of Computational Physics, 161(2):484–511. https://doi.org/10.1006/jcph.2000.6507

Nathanail A, Mpisketzis V, Porth O, et al (2022) Monthly Notices of the Royal Astronomical Society, 513(3):4267–4277. https://doi.org/10.1093/mnras/stac1118, [astro-ph.HE]

Øieroset M, Lin RP, Phan TD, et al (2002) Physical Review Letters, 89(19):195001. https://doi.org/10.1103/PhysRevLett.89.195001

Oka M, Phan TD, Krucker S, et al (2010) Astrophysical Journal, 714(1):915–926. https://doi.org/10.1088/0004-637X/714/1/915, [astro-ph.SR]

Oka M, Birn J, Egedal J, et al (2023) arXiv e-prints, arXiv:2307.01376. https://doi.org/10.48550/arXiv.2307.01376, [physics.space-ph]

Palenzuela C, Lehner L, Reula O, et al (2009) Monthly Notices of the

Royal Astronomical Society, 394(4):1727–1740. https://doi.org/10.1111/j.1365-2966.2009.14454.x, [astro-ph]

Palenzuela C, Lehner L, Ponce M, et al (2013) Physical Review Letters, 111(6):061105. https://doi.org/10.1103/PhysRevLett.111.061105, [gr-qc]

Parker EN (1957) Journal of Geophysical Research, 62(4):509–520. https://doi.org/10.1029/JZ062i004p00509

Parker EN (1965) Planetary and Space Science, 13(1):9–49. https://doi.org/10.1016/0032-0633(65)90131-5

Petropoulou M, Sironi L (2018) Monthly Notices of the Royal Astronomical Society, 481(4):5687–5701. https://doi.org/10.1093/mnras/sty2702

Petropoulou M, Giannios D, Sironi L (2016) Monthly Notices of the Royal Astronomical Society, 462(3):3325–3343. https://doi.org/10.1093/mnras/stw1832

Petschek HE (1964) Magnetic Field Annihilation. In: Proceedings of the AAS-NASA Symposium, vol 50. NASA Special Publication, p 425

Philippov A, Kramer M (2022) Annual Review of Astronomy and Astrophysics, 60:495–558. https://doi.org/10.1146/annurev-astro-052920-112338

Philippov A, Uzdensky DA, Spitkovsky A, et al (2019) Astrophysical Journal Letters, 876(1):L6. https://doi.org/10.3847/2041-8213/ab1590

Pritchett PL (2001) Journal of Geophysical Research, 106(A3):3783–3798. https://doi.org/10.1029/1999JA001006

Remillard RA, McClintock JE (2006) Annual Review of Astronomy and Astrophysics, 44(1):49–92. https://doi.org/10.1146/annurev.astro.44.051905.092532, [astro-ph]

Ripperda B, Bacchini F, Porth O, et al (2019) Astrophysical Journal Supplementary, 244(1):10. https://doi.org/10.3847/1538-4365/ab3922, [physics.comp-ph]

Ripperda B, Bacchini F, Philippov AA (2020) Astrophysical Journal, 900(2):100. https://doi.org/10.3847/1538-4357/ababab

Schoeffler KM, Grismayer T, Uzdensky D, et al (2019) Astrophysical Journal, 870(1):49. https://doi.org/10.3847/1538-4357/aaf1b9, [astro-ph.HE]

Schoeffler KM, Grismayer T, Uzdensky D, et al (2023) Monthly Notices of the Royal Astronomical Society, 523(3):3812–3839. https://doi.org/10.1093/mnras/stad1588, [astro-ph.HE]

Seo J, Ryu D, Kang H (2022) arXiv e-prints, arXiv:2212.04159. https://doi.org/10.48550/arXiv.2212.04159, [astro-ph.HE]

Shibata K, Tanuma S (2001a) Earth, Planets and Space, 53:473–482. https://doi.org/10.1186/BF03353258, [astro-ph]

Shibata K, Tanuma S (2001b) Earth, Planets and Space, 53:473–482. https://doi.org/10.1186/BF03353258, [astro-ph]

Sironi L (2022) Physical Review Letters, 128(14):145102. https://doi.org/10.1103/PhysRevLett.128.145102

Sironi L, Beloborodov AM (2020) Astrophysical Journal, 899(1):52. https://doi.org/10.3847/1538-4357/aba622

Sironi L, Spitkovsky A (2011) Astrophysical Journal, 741(1):39. https://doi.org/10.1088/0004-637X/741/1/39

Sironi L, Spitkovsky A (2014) Astrophysical Journal Letters, 783(1):L21. https://doi.org/10.1088/2041-8205/783/1/L21

Sironi L, Petropoulou M, Giannios D (2015) Monthly Notices of the Royal Astronomical Society, 450(1):183–191. https://doi.org/10.1093/mnras/stv641

Sironi L, Giannios D, Petropoulou M (2016) Monthly Notices of the Royal Astronomical Society, 462(1):48–74. https://doi.org/10.1093/mnras/stw1620

Spitkovsky A (2008) Astrophysical Journal Letters, 673(1):L39. https://doi.org/10.1086/527374, [astro-ph]

Spruit HC (2010) Theory of Magnetically Powered Jets. In: Belloni T (ed) Lecture Notes in Physics, vol 794. Berlin Springer Verlag, p 233, https://doi.org/10.1007/978-3-540-76937-8_9

Stanier A, Daughton W, Le A, et al (2019) Physics of Plasmas, 26(7):072121. https://doi.org/10.1063/1.5100737, [physics.plasm-ph]

Sugiyama T, Kusano K (2007) Journal of Computational Physics, 227(2):1340–1352. https://doi.org/10.1016/j.jcp.2007.09.011

Sun X, Bai XN (2023) Monthly Notices of the Royal Astronomical Society, 523(3):3328–3347. https://doi.org/10.1093/mnras/stad1548, [astro-ph.HE]

Sweet PA (1958) Il Nuovo Cimento, 8(S2):188–196. https://doi.org/10.1007/BF02962520

Takahashi HR, Ohsuga K (2013) Astrophysical Journal, 772(2):127. https://doi.org/10.1088/0004-637X/772/2/127

Takahashi HR, Kudoh T, Masada Y, et al (2011) Astrophysical Journal Letters, 739(2):L53. https://doi.org/10.1088/2041-8205/739/2/L53

Takamoto M (2013) Astrophysical Journal, 775(1):50. https://doi.org/10.1088/0004-637X/775/1/50

Takamoto M, Inoue T (2011) Astrophysical Journal, 735(2):113. https://doi.org/10.1088/0004-637X/735/2/113

Tavani M, Bulgarelli A, Vittorini V, et al (2011) Science, 331(6018):736. https://doi.org/10.1126/science.1200083, [astro-ph.HE]

Tenerani A, Velli M, Pucci F, et al (2016) Journal of Plasma Physics, 82(5):535820501. https://doi.org/10.1017/S002237781600088X, [astro-ph.SR]

Tsallis C (1988) Journal of Statistical Physics, 52(1-2):479–487. https://doi.org/10.1007/BF01016429

Usami S, Horiuchi R, Ohtani H, et al (2013) Physics of Plasmas, 20(6):061208. https://doi.org/10.1063/1.4811121

Uzdensky DA (2011) Space Science Reviews, 160(1-4):45–71. https://doi.org/10.1007/s11214-011-9744-5

Uzdensky DA (2016) Radiative Magnetic Reconnection in Astrophysics. In: Gonzalez W, Parker E (eds) Magnetic Reconnection: Concepts and Applications, p 473, https://doi.org/10.1007/978-3-319-26432-5_12, 1510.05397

Uzdensky DA (2022) Journal of Plasma Physics, 88(1):905880114. https://doi.org/10.1017/S0022377822000046, [astro-ph.HE]

Uzdensky DA, Loureiro NF (2016) Physical Review Letters, 116(10):105003. https://doi.org/10.1103/PhysRevLett.116.105003, [astro-ph.SR]

Uzdensky DA, Spitkovsky A (2014) Astrophysical Journal, 780(1):3. https://doi.org/10.1088/0004-637X/780/1/3

Uzdensky DA, Loureiro NF, Schekochihin AA (2010) Physical Review Letters, 105(23):235002. https://doi.org/10.1103/PhysRevLett.105.235002, [astro-ph.SR]

Uzdensky DA, Cerutti B, Begelman MC (2011) Astrophysical Journal Letters, 737(2):L40. https://doi.org/10.1088/2041-8205/737/2/L40

Vasyliunas VM (1968) Journal of Geophysical Research, 73(9):2839–2884. https://doi.org/10.1029/JA073i009p02839

Watanabe N, Yokoyama T (2006) Astrophysical Journal Letters, 647(2):L123–L126. https://doi.org/10.1086/507520, [astro-ph]

Webb GM (1989) Astrophysical Journal, 340:1112. https://doi.org/10.1086/167462

Werner GR, Uzdensky DA, Cerutti B, et al (2016) Astrophysical Journal Letters, 816(1):L8. https://doi.org/10.3847/2041-8205/816/1/L8

Werner GR, Uzdensky DA, Begelman MC, et al (2018) Monthly Notices of the Royal Astronomical Society, 473(4):4840–4861. https://doi.org/10.1093/mnras/stx2530

Werner GR, Philippov AA, Uzdensky DA (2019) Monthly Notices of the Royal Astronomical Society, 482(1):L60–L64. https://doi.org/10.1093/mnrasl/sly157, [astro-ph.HE]

Yang H, Yuan F, Li H, et al (2022) arXiv e-prints, arXiv:2206.05661. https://doi.org/10.48550/arXiv.2206.05661

Yang L, Li H, Guo F, et al (2020) Astrophysical Journal Letters, 901(2):L22. https://doi.org/10.3847/2041-8213/abb76b, [astro-ph.SR]

Zank GP (2014) Transport Processes in Space Physics and Astrophysics, vol 877. Springer, https://doi.org/10.1007/978-1-4614-8480-6

Zanotti O, Dumbser M (2011) Monthly Notices of the Royal Astronomical Society, 418(2):1004–1011. https://doi.org/10.1111/j.1365-2966.2011.19551.x

Zenitani S (2018) Plasma Physics and Controlled Fusion, 60(1):014028. https://doi.org/10.1088/1361-6587/aa8f17

Zenitani S, Hoshino M (2001) Astrophysical Journal Letters, 562(1):L63–L66. https://doi.org/10.1086/337972

Zenitani S, Hoshino M (2005a) Astrophysical Journal Letters, 618(2):L111–L114. https://doi.org/10.1086/427873, [astro-ph]

Zenitani S, Hoshino M (2005b) Physical Review Letters, 95(9):095001. https://doi.org/10.1103/PhysRevLett.95.095001, [astro-ph]

Zenitani S, Hoshino M (2007) Astrophysical Journal, 670(1):702–726. https://doi.org/10.1086/522226, [astro-ph]

Zenitani S, Hoshino M (2008) Astrophysical Journal, 677(1):530–544. https://doi.org/10.1086/528708, [astro-ph]

Zenitani S, Hesse M, Klimas A (2009a) Astrophysical Journal, 696(2):1385–1401. https://doi.org/10.1088/0004-637X/696/2/1385

Zenitani S, Hesse M, Klimas A (2009b) Astrophysical Journal, 705(1):907–913. https://doi.org/10.1088/0004-637X/705/1/907

Zenitani S, Hesse M, Klimas A (2010) Astrophysical Journal Letters, 716(2):L214–L218. https://doi.org/10.1088/2041-8205/716/2/L214

Zhang B, Yan H (2011) Astrophysical Journal, 726(2):90. https://doi.org/10.1088/0004-637X/726/2/90

Zhang H, Giannios D (2021) Monthly Notices of the Royal Astronomical Society, 502(1):1145–1157. https://doi.org/10.1093/mnras/stab008

Zhang H, Chen X, Böttcher M, et al (2015) Astrophysical Journal, 804(1):58. https://doi.org/10.1088/0004-637X/804/1/58, [astro-ph.HE]

Zhang H, Li H, Guo F, et al (2017) Astrophysical Journal, 835(2):125. https://doi.org/10.3847/1538-4357/835/2/125

Zhang H, Li X, Guo F, et al (2018) Astrophysical Journal Letters, 862(2):L25. https://doi.org/10.3847/2041-8213/aad54f

Zhang H, Li X, Giannios D, et al (2020) Astrophysical Journal, 901(2):149. https://doi.org/10.3847/1538-4357/abb1b0

Zhang H, Li X, Giannios D, et al (2021a) Astrophysical Journal, 912(2):129. https://doi.org/10.3847/1538-4357/abf2be

Zhang H, Sironi L, Giannios D (2021b) Astrophysical Journal, 922(2):261. https://doi.org/10.3847/1538-4357/ac2e08, [astro-ph.HE]

Zhang H, Li X, Giannios D, et al (2022a) Astrophysical Journal, 924(2):90. https://doi.org/10.3847/1538-4357/ac3669

Zhang H, Sironi L, Giannios D, et al (2023) arXiv e-prints, arXiv:2302.12269. https://doi.org/10.48550/arXiv.2302.12269, [astro-ph.HE]

Zhang Q, Guo F, Daughton W, et al (2021c) Physical Review Letters, 127(18):185101. [astro-ph.SR]

Zhang Q, Guo F, Daughton W, et al (2022b) arXiv e-prints, arXiv:2210.04113. https://doi.org/10.48550/arXiv.2210.04113, [astro-ph.SR]

Zrake J (2016) Astrophysical Journal, 823(1):39. https://doi.org/10.3847/0004-637X/823/1/39

Zweibel EG, Yamada M (2009) Annual Review of Astronomy and Astrophysics, 47(1):291–332. https://doi.org/10.1146/annurev-astro-082708-101726